NeuroImage 237 (2021) 118187

Contents lists available at ScienceDirect

NeuroImage

journal homepage: www.elsevier.com/locate/neuroimage

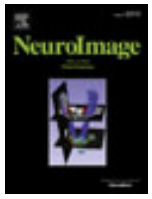

The coupling of BOLD signal variability and degree centrality underlies cognitive functions and psychiatric diseases

Jintao Sheng[a], Liang Zhang[a], Junjiao Feng[a], Jing Liu[a], Anqi Li[a], Wei Chen[b], Yuedi Shen[c], Jinhui Wang[d,e], Yong He[a], Gui Xue[a,*]

[a] State Key Laboratory of Cognitive Neuroscience and Learning & IDG/McGovern Institute of Brain Research, Beijing Normal University, Beijing 100875, PR China
[b] Department of Psychiatry, Sir Run Run Shaw Hospital, Zhejiang University School of Medicine, and the Collaborative Innovation Center for Brain Science, Hangzhou, Zhejiang 310000, PR China
[c] The Affiliated Hospital of Hangzhou Normal University, Hangzhou Normal University, Hangzhou, Zhejiang 310000, PR China
[d] Guangdong Key Laboratory of Mental Health and Cognitive Science, Center for Studies of Psychological Application, South China Normal University, Institute for Brain Research and Rehabilitation, Guangzhou 510631, PR China
[e] Key Laboratory of Brain, Ministry of Education, Cognition and Education Sciences (South China Normal University), PR China

ARTICLE INFO

Keywords:
Resting-state fMRI
Mean-scaled fractional BOLD signal variability
Degree centrality
Cognitive function
Disease vulnerability

ABSTRACT

Brain signal variability has been consistently linked to functional integration; however, whether this coupling is associated with cognitive functions and/or psychiatric diseases has not been clarified. Using multiple multi-modality datasets, including resting-state functional magnetic resonance imaging (rsfMRI) data from the Human Connectome Project (HCP: $N = 927$) and a Beijing sample ($N = 416$) and cerebral blood flow (CBF) and rsfMRI data from a Hangzhou sample ($N = 29$), we found that, compared with the existing variability measure (i.e., SD_{BOLD}), the mean-scaled (standardized) fractional standard deviation of the BOLD signal ($mfSD_{BOLD}$) maintained very high test-retest reliability, showed greater cross-site reliability and was less affected by head motion. We also found strong reproducible couplings between the $mfSD_{BOLD}$ and functional integration measured by the degree centrality (DC), both cross-voxel and cross-subject, which were robust to scanning and preprocessing parameters. Moreover, both $mfSD_{BOLD}$ and DC were correlated with CBF, suggesting a common physiological basis for both measures. Critically, the degree of coupling between $mfSD_{BOLD}$ and long-range DC was positively correlated with individuals' cognitive total composite scores. Brain regions with greater mismatches between $mfSD_{BOLD}$ and long-range DC were more vulnerable to brain diseases. Our results suggest that BOLD signal variability could serve as a meaningful index of local function that underlies functional integration in the human brain and that a strong coupling between BOLD signal variability and functional integration may serve as a hallmark of balanced brain networks that are associated with optimal brain functions.

Introduction

Cognitive functions depend on an advanced functional system that requires a dynamic, context-sensitive balance between functional integration and segregation in the brain (Chan et al., 2017; Fornito et al., 2012; Shine et al., 2018). Consistently, it has been revealed that anatomically separated brain regions fluctuate synchronously and show strong functional connectivity (FC), thus forming a complex functional network (Biswal et al., 1995). Among this network, some regions, such as the posterior cingulate, lateral temporal, lateral parietal, and medial/lateral prefrontal cortices, have disproportionately higher numbers of connections and act as brain hubs to integrate diverse informational sources and balance functional integration and segregation in the brain (Buckner et al., 2009; Sporns et al., 2007). Given the important role of brain hubs in functional networks and their vulnerability to diseases (Buckner et al., 2009; Khan et al., 2013; Liu et al., 2015; Sheng et al., 2018; Yan et al., 2019), many studies have tried to determine the anatomical, physiological, and metabolic basis of their connectivity. For example, the FC between different brain regions corresponds well with their nerve fibre connectivity (Greicius et al., 2009; Honey et al., 2009), indicating a strong anatomical basis for FC. In addition, FC has also been shown to be closely related to regional cerebral blood flow (CBF) and metabolism, such that highly connected hub regions showed greater regional CBF (Liang et al., 2013), higher oxygen consumption (Wu et al., 2009) and glucose metabolism (Tomasi et al., 2013).

In addition to the anatomical and metabolic basis of FC, a growing body of research has suggested that FC is also related to the

* Corresponding author.
E-mail address: gxue@bnu.edu.cn (G. Xue).

https://doi.org/10.1016/j.neuroimage.2021.118187.
Received 23 August 2020; Received in revised form 16 May 2021; Accepted 17 May 2021
Available online 19 May 2021.

dynamic changes (or variability) of local neuronal ensemble activities, which reflect the neural flexibility (Nomi et al., 2017), or the dynamic range that affects the adaptability and efficiency of neural systems (Garrett et al., 2013b). First, developmental studies have revealed that both FC (Cao et al., 2017; Toulmin et al., 2015) and brain signal variability (McIntosh et al., 2008; Vakorin et al., 2011) increase with age, although elderly subjects show reduced FC (Damoiseaux, 2017; Ferreira and Busatto, 2013) and signal variability (Armbruster-Genc et al., 2016; Garrett et al., 2010,2011, 2013a). Second, individuals with stroke (Kielar et al., 2016), multiple sclerosis (Petracca et al., 2017), Alzheimer's disease (Scarapicchia et al., 2018) and other neurological disorders (Zoller et al., 2017) have regional neural variability abnormalities and accompanying brain network dysfunction (Colasanti et al., 2016; Dennis and Thompson, 2014). Third, dopamine and other neurotransmitters could boost signal variability (Alavash et al., 2018; Garrett et al., 2015) and increase FC (Alavash et al., 2018; Kelly et al., 2009; Nagano-Saito et al., 2008).

Several studies have directly examined the coupling of signal variability and FC using different brain image data and measures of signal variability. For example, one electroencephalography (EEG) study used multiscale entropy (MSE) to measure signal variability and revealed positive correlations between MSE and FC (Misic et al., 2011). Using the blood oxygen level-dependent (BOLD) signal and amplitude of low-frequency fluctuation (ALFF) or fractional ALFF (fALFF) to measure brain signal variability, several studies revealed that fALFF/ALFF (f/ALFF) was positively correlated with FC (Di et al., 2013; Sato et al., 2019; Tomasi et al., 2016; Yan et al., 2017). The variability of BOLD signals could be measured by the resting state fluctuation amplitude (RSFA) (Kannurpatti and Biswal, 2008) or temporal standard deviation (SD_{BOLD}) (Garrett et al., 2010; Nomi et al., 2017), and a recent study observed that greater SD_{BOLD} values were associated with lower functional network dimensionality within functional networks, suggesting that local variability in BOLD signals is related to information communication (Garrett et al., 2018).

Previous studies have led to several important questions that deserve further investigation. First, most of the above studies either examined coupling across subjects or at the group level, and very few studies have examined coupling across voxels (but see Yan et al., 2017). Second, considering the replication crisis in neuroimaging literature, it is important to use a large dataset and to examine the reliability of this coupling across both scanning sessions and different sites. Finally, and most importantly, previous studies have not examined the individual differences in the coupling between BOLD signal variability and FC; thus, the functional relevance of this coupling is unknown.

The current study aimed to address these questions using large resting-state functional magnetic resonance imaging (rsfMRI) samples from different scanners and acquisition parameters. It should be noted that most variability measures, such as SD_{BOLD}, ALFF or RSFA, are affected by factors that include the echo time (TE) and the initial BOLD signal strength (S_0, when the TE = 0) (Evans et al., 2015), which increases the difficulty of comparing results from different scanners and acquisition parameters. To improve the cross-scanner reliability, we used a new brain signal variability measure, i.e., the mean-scaled fractional standard deviation of BOLD signal ($mfSD_{BOLD}$), which was based on a previous study (Zou et al., 2008). As a result, the first part of the current study was to compare the stability and reliability of measures of BOLD signal variability and explored the relationships among the BOLD signal variability, degree centrality (DC, a measure of FC strength) and CBF.

In the second part, we further examined the functional relevance of the coupling between BOLD signal variability and DC, which were both positively correlated with CBF. First, we systematically examined the reliability of cross-voxel and cross-subject couplings between $mfSD_{BOLD}$ and DC across different scanning sessions, datasets, and processing parameters. Second, we investigated the functional relevance of this coupling by exploring the association between coupling strength and individuals' cognitive function. Third, we further examined whether the degree of decoupling between $mfSD_{BOLD}$ and DC was associated with disease vulnerability. We hypothesized that the variability of BOLD signals and degree centrality were tightly coupled, and that the degree of coupling was related to cognitive function and susceptibility to brain diseases.

Materials and Methods

Three datasets were used in this study. The primary data were obtained from the publicly available Human Connectome Project (HCP) ($N = 927$). The other two validation datasets were acquired from Beijing Normal University ($N = 416$) and Hangzhou Normal University ($N = 29$). All participants were healthy adults. These three datasets are described in detail below.

2.1. HCP dataset: participants and data preprocessing

We used rsfMRI data from the 1200 Subjects Release (S1200) dataset of the HCP (Van Essen et al., 2013). A total of 927 subjects (434 males; age = 22–35 years old, mean age = 28.60 years old) were used for analyzes after excluding participants who did not finish both sessions (REST1 and REST2) ($N = 176$), those with incomplete fMRI data (the number of volumes was smaller than 1200) ($N = 21$), those with excessive head motion (mean framewise displacement, mFD > 0.3, $N = 51$) or those without cognitive total composite scores ($N = 11$). We also excluded participants aged 36 years old and above ($N = 13$) to increase the age homogeneity. To reduce the potential influence of encoding directions, we only used the two rsfMRI scans with a left-to-right (LR) phase-encoding direction. To rule out the influence of twins and siblings (McDonough and Siegel, 2018), a subgroup of 356 unrelated participants (170 males; age = 22–35 years old, mean age = 28.42 years old) were randomly selected from the 927 participants to verify the results. Each rsfMRI run was acquired at 2 mm isotropic resolution with a repetition time of 720 ms and lasted for 14 min and 33 s. For details of the data acquisition parameters, see Smith et al. (2013).

The extensive preprocessing pipeline was performed by the HCP team (Smith et al., 2013), which includes echo-planar imaging gradient distortion correction, motion correction, field bias correction, spatial transformation into common Montreal Neurological Institute (MNI) space (Glasser et al., 2013), and artefact removal using independent component analysis (ICA) with the MELODIC and FIX tools implemented in FSL (Griffanti et al., 2014; Salimi-Khorshidi et al., 2014). We additionally constructed a single regression model to simultaneously perform nuisance regression (including the mean white matter (WM), cerebrospinal fluid (CSF), and global signal time series) and bandpass (0.01–0.1 Hz)/high-pass (> 0.01 Hz) filtering (Lindquist et al., 2019) using the 3dTproject function (Caballero-Gaudes and Reynolds, 2017) provided by Analysis of Functional NeuroImage (AFNI) (Cox, 1996). To examine the effect of global signal regression on the results, we performed another analysis using the model described above but without global signal regression.

2.2. Beijing dataset: participants, data acquisition and preprocessing

A total of 493 healthy Chinese college students were recruited as a part of the Cognitive Neurogenetic Study of Chinese Young Adults (CNSCYA) Project (Feng et al., 2020). All of them had normal or corrected-to-normal vision and no history of psychiatric or neurological diseases. Written consent was obtained from each participant after he/she received a full explanation of the study procedure. Seventy-seven participants were excluded due to excessive head motion (mFD > 0.3) ($N = 43$) or incomplete cerebellar coverage ($N = 34$). The final sample consisted of 416 participants (186 males; age = 17–29 years; mean age = 21.5 years). The study was approved by the Institutional Review Board at Beijing Normal University.

MRI data acquisition: Imaging data were acquired using a 3.0 T Siemens MRI scanner (Siemens Medical Systems, Erlangen, Germany) in the Brain Imaging Center at Beijing Normal University. Resting-state fMRI images were acquired using the Gradient Echo Type Echo-Planar Imaging (GRE-EPI) sequence. The acquisition parameters were as follows: TR/TE = 2000 ms/30 ms, flip angle (FA) = 90°, resolution matrix = 64 × 64, FOV = 200 × 200 mm^2, thickness = 3.5 mm, and acquisition voxel size = 3.1 × 3.1 × 3.5 mm^3. A total of 33 transverse slices were used to cover the whole brain. A total of 200 volumes were collected in a 6 min and 40 s scan, during which all participants were instructed to relax and keep their eyes closed but not to sleep (Damoiseaux et al., 2006). The anatomical scan was acquired using the T1-weighted magnetization prepared rapid acquisition gradient-echo (MPRAGE) sequence with the following parameters: inversion time (TI) = 1100 ms; TR/TE/FA = 2530 ms/3.39 ms/7°, FOV = 256 × 256 mm^2, matrix = 192 × 256, slice thickness = 1.33 mm, 144 sagittal slices, and voxel size = 1.3 × 1.0 × 1.3 mm^3.

fMRI data processing. All fMRI data were processed using FSL (www.fmrib.ox.ac.uk/fsl), SPM12 (www.fil.ion.ucl.ac.uk/spm/software/spm12/), GRETNA (Wang et al., 2015), AFNI (https://afni.nimh.nih.gov/), R 4.0.2 (R. Core Team, 2020) and custom MATLAB (R2017a) codes unless stated otherwise.

The first 5 volumes of each participant were removed to allow for T1 equilibration effects. The remaining 195 volumes were then corrected for intervolume head motion (six-parameter rigid-body transformation), intravolume temporal offsets (sinc interpolation) and high-pass filtered (> 0.01 Hz). Data were then smoothed using a 6-mm Gaussian kernel. Subsequently, we implemented ICA denoising using the same approach as that used in the HCP dataset. Specifically, the classifier was trained on a small training set (20 participants). We first manually classified the "bad" components according to several primary criteria proposed by Griffanti et al. (2017). The training set was then used in a quadratic classifier to automatically separate components into artefact and nonartefact categories and applied to the new dataset. The identified artefact components were then filtered out from the corresponding fMRI data. All resulting images were spatially normalized to standard MNI space using DARTEL implemented in SPM and resampled to 3 × 3 × 3 mm^3 resolution. Finally, we performed the same nuisance regression and band-pass filtering that was performed on the HCP dataset.

2.3. Hangzhou dataset: participants, data acquisition and preprocessing

To examine the relationship among BOLD signal variability, CBF and FC, we analyzed another Hangzhou dataset with resting-state BOLD fMRI images and arterial spin labeling (ASL) fMRI images (Sheng et al., 2018). Twenty-nine healthy right-handed participants were included in the current study (5 males; age = 23–66 years; mean age = 42.31 years). This study was approved by the Ethics Committee of the Sir Run Run Shaw Hospital, School of Medicine, Zhejiang University, and the Affiliated Hospital of Hangzhou Normal University. All participants provided written informed consent.

MRI data acquisition: All MRI data were acquired using a 3.0 T MR scanner (GE Discovery MR750, GE Medical Systems, Milwaukee, WI) equipped with an eight-channel head coil array. The resting-state ASL MRI data were acquired with a 3D pseudo-continuous arterial spin labeling sequence: 72 axial slices, TR/TE = 4632 ms/10.5 ms, FOV = 240 × 240 mm^2, matrix = 128 × 128, slice thickness = 4 mm, no gap, number of excitations = 3 and post-labeling delay = 1525 ms. The resting-state BOLD fMRI data were obtained axially using a single-shot, gradient-recalled echo-planar imaging sequence parallel to the line of the anterior-posterior commissure. The acquisition parameters were as follows: 37 slices, TR/TE/FA = 2000 ms/30 ms/90°, field of view (FOV) = 220 × 220 mm^2, matrix = 128 × 128, slice thickness = 3.2 mm and no gap. A total of 184 volumes were acquired for each participant. High-resolution T1-weighted images were also acquired for each participant with a three-dimensional spoiled gradient-recalled sequence: 176 axial slices, TR/TE/FA = 8.1 ms/3.1 ms/8°, FOV = 250 × 250 mm^2, matrix = 256 × 256, slice thickness = 1.0 mm and no gap.

MRI data processing. The rsfMRI data were processed with the same procedures as those used on the Beijing dataset. For the ASL MRI data, individual CBF images were first obtained using Functool (version 12.2.01), an automated image postprocessing tool embedded in the GE healthcare MR-750 system. To correct for the partial volume effects (PVEs) introduced by the large voxel size used in ASL MRI, participants' structural images were segmented into grey matter (GM), WM, and CSF using SPM12. The corresponding GM, WM, and CSF probability maps were then registered and resampled to the native ASL MRI space using an inter-modality registration algorithm that uses normalized mutual information as the objective function. The PET-based method was then used to correct PVEs (Hu et al., 2010; Wang et al., 2008). Finally, the PVE-corrected CBF images were spatially normalized to standard MNI space (using the transformation fields derived from the tissue segmentation data of structural images), resampled to 3 mm isotropic voxels, and spatially smoothed (Gaussian kernel with full width at half maximum (FWHM) = 6 mm).

2.4. Calculation of DC, SD_{BOLD} and $mfSD_{BOLD}$

After the above preprocessing steps, we calculated the voxelwise full/long-range DC, SD_{BOLD} and fSD_{BOLD}/$mfSD_{BOLD}$ (m/fSD_{BOLD}).

The DC quantifies the overall connectivity of a node to all other nodes in a network. Briefly, for a given voxel, its time series were extracted and correlated with the time series of all other voxels in the brain. To improve the normality of the correlations, we transformed the correlation coefficients to Z-scores using Fisher's r-to-Z transformation. The summation of the resulting Fisher's Z-score across all other voxels was then calculated and assigned to this given voxel. To exclude the confounding effects of spurious correlations, correlation coefficients smaller than a cut-off threshold *r* were excluded prior to the summation. To make the network sparsity level comparable across different datasets, we used different cut-off correlation thresholds to calculate DC for different datasets (Table S1). Negative correlations were excluded due to their ambiguous interpretation (Fox et al., 2009; Murphy et al., 2009). For full-range DC, correlations with spatially close voxels (Euclidean distance < 20 mm) were excluded (Power et al., 2011). These correlations were excluded to avoid the influence of possible shared signals between nearby voxels on DC and to minimize the effects of data processing (e.g., blurring, reslicing) and head motion on DC (Power et al., 2012). Additionally, we calculated the long-range DC, which only included the correlations with voxels that had an anatomical distance of more than 75 mm (Achard et al., 2006; He et al., 2007) with a given voxel, allowing us to further explore the effects of anatomical distance in this study. Furthermore, we examined the impact of the global signal (without global signal regression, NGSR) and the network type (binary network, defined by an adjacent matrix using one (the edges that survived the abovementioned cut-off threshold *r*) and zero (edges below threshold)) (Bullmore and Sporns, 2009) on the results using the HCP dataset.

The SD_{BOLD} for each voxel was quantified as the standard deviation across the time series of low-frequency ($0.01 < f < 0.1$ Hz) signals (Garrett et al., 2018), which reflected the extent of the BOLD signal changes over time. To minimize the effects of the initial BOLD signal strength (S_0, which is principally altered by structural noise sources) (Power et al., 2018) and TE (Evans et al., 2015), following Zou et al. (2008), we also calculated the fSD_{BOLD}, which was quantified as the low-frequency (0.01–0.1 Hz) SD_{BOLD} divided by the high-pass filtering frequency (> 0.01 Hz) SD_{BOLD}. Furthermore, we calculated the mean-scaled (standardized) fSD_{BOLD} ($mfSD_{BOLD}$) to minimize the effects of in-scanner head movements and global effects by dividing the fSD_{BOLD} of each voxel by the mean fSD_{BOLD} of the whole brain (Kublbock et al., 2014).

The resultant DC, SD_{BOLD} and m/fSD_{BOLD} maps were further spatially smoothed with a 5 mm Gaussian kernel for the HCP dataset only because the Beijing and Hangzhou data were already smoothed during preprocessing. Unless otherwise specified, the results of the HCP data were obtained based on the average of the two sessions (REST1 and REST2). Notably, all the DC, SD_{BOLD} and m/fSD_{BOLD} calculations were restricted within dataset-specific brain masks derived according to the following two criteria: (a) nonzero variance of BOLD signals for all participants and (b) > 20% grey matter tissue probability based on the tissue probability map attained using the SPM12 package.

2.5. Statistical analysis

2.5.1. Stability and reliability of BOLD signal variability

To examine the stability and reliability of the variability of BOLD signals, we calculated the Pearson correlation coefficient and intraclass correlation coefficient (ICC) across sessions (REST1 and REST2 for the HCP dataset), different datasets (HCP, Beijing, and Hangzhou), different cut-off thresholds (0.05, 0.075, 0.10 and 0.15) for DC calculations (HCP dataset), and different data processing strategies, such as network binarization and without global signal regression (HCP dataset). Using psych and lme4 packages in R 4.0.2, the ICC was calculated by fitting linear mixed-effects models based on the following formula (Shrout and Fleiss, 1979):

$$ICC = (MSB - MSE)/MSB$$

where *MSB* is the between-target mean square and *MSE* is the mean square of errors. An *ICC* value greater than 0.4 is commonly expected in practice (Zuo and Xing, 2014).

Due to the different spatial resolutions and brain coverage across datasets, the spatial pattern similarity of the three datasets could not be examined at the voxel level. Thus, the Fan 246 template (Fan et al., 2016) was used to extract the signals in each brain region, which were then used to calculate the cross-site reliability. We retained 222 regions of interest (ROIs) that were shared by all participants in all three datasets. In addition, the Yeo 2011 template (Yeo et al., 2011) with 114 parcels (108 remaining parcels after combining all three datasets) was used to verify this result.

In a further analysis, we examined the cross-site reliability/ICC within each brain region. First, the group-averaged BOLD signal variability maps of the HCP dataset were first resampled to 3 mm resolution. Then, we calculated their cross-site reliability at each brain region based on the Fan 246 template (Fan et al., 2016). Since the number of voxels was different in each brain region, we restricted our analysis to regions with at least 50 voxels (170 ROIs). For the regions with more than 50 voxels, 50 voxels were randomly selected from each region to calculate the ICC, and this process was repeated 1000 times. The cross-site reliability for each brain region was obtained by averaging the ICCs from the 1000 repetitions.

2.5.2. Correlations among $mfSD_{BOLD}$, DC and CBF

Pearson correlation analyzes were performed to examine the cross-subject or cross-voxel relationship among $mfSD_{BOLD}$, DC and CBF. Neighboring voxels were spatially dependent mainly because of spatial smoothing (Xiong et al., 1995); thus, the effective degree of freedom (df_{eff}) was corrected by the following formula (Liang et al., 2013):

$$df_{eff} = N/\left(FWHM_X \times FWHM_Y \times FWHM_Z\right)/v - 2$$

where v is the nominal volume of the voxels, N is the number of voxels used in the analysis, and *FWHM* represents the spatial smoothness estimated by using AFNI's 3dFWHMx. The df_{eff} result was then used to estimate the p values for the cross-voxel correlation analyzes. For the cross-subject correlation analyzes, we controlled for age, sex, age^2, age × sex, age^2 × sex and mFD.

2.5.3. Functional relevance of the coupling between $mfSD_{BOLD}$ and DC

The coupling between DC and $mfSD_{BOLD}$ was defined based on their correlation coefficient, with a higher correlation indicating tighter coupling. Before examining the functional relevance of DC-$mfSD_{BOLD}$ coupling, the individual correlation coefficients were transformed to Fisher's Z-scores to improve the normality of the correlations and to facilitate further statistical tests.

Age and sex differences in DC-$mfSD_{BOLD}$ coupling. To examine the age (22-35 years) and sex (male and female) effects of the coupling, we performed linear least-squares regression in R 4.0.2, with age, sex, and age by sex interaction as independent variables and mFD as a covariant.

DC-$mfSD_{BOLD}$ coupling and cognitive performance. We used the cognitive total composite scores (CogTotalComp) in the HCP dataset to quantify individuals' cognitive performance (Van Essen et al., 2013). The scores were derived by averaging the normalized scores of each of the fluid and crystallized cognition measures, which were then converted to standardized scores using the following formula: $\frac{x-\bar{x}}{S} \times 15 + 100$, where $\bar{x}$ is the sample mean of the averaged normalized scores and S is the sample standard deviation of the averaged normalized scores. Partial correlation analyzes were performed to examine the relationship between DC-$mfSD_{BOLD}$ coupling (correlation coefficient) and cognitive total composite scores, with age, sex, age^2, age × sex, age^2 × sex and mFD as control variables. Permutation tests (N = 10,000) were performed to test the significance of the R values.

DC-$mfSD_{BOLD}$ mismatch and cognitive performance. The DC and $mfSD_{BOLD}$ values were first separately Z-transformed, and a least-squares linear regression model was then applied to fit the DC and $mfSD_{BOLD}$ results across voxels for each participant. Residuals that could not be explained by $mfSD_{BOLD}$ were used as a measurement of DC-$mfSD_{BOLD}$ mismatch, with a higher absolute value of the DC residual reflecting a greater mismatch between DC and $mfSD_{BOLD}$. Subsequently, for a given voxel, a partial correlation analysis was conducted between the individuals' absolute DC residuals and the cognitive total composite scores, controlling age, sex, age^2, age × sex, age^2 × sex and mFD, and this analysis was performed in DPABI (Yan et al., 2016). The permutation test (N = 1000) with threshold-free cluster enhancement (TFCE) was used to correct whole-brain multiple comparisons, which achieved the best balance between the familywise error rate (< 5%) and test-retest (TRT) reliability (Chen et al., 2018; Winkler et al., 2016).

DC-$mfSD_{BOLD}$ mismatch and disease susceptibility. To explore whether brain regions exhibiting greater mismatch were also more vulnerable to brain diseases, we adopted the disease-susceptible areas from a previous study (Sha et al., 2018). Notably, there were two disorder-general activation likelihood estimation (ALE) maps, with one indicating the probability of reduced activity (i.e., disorders < controls; Fig. 6A, left) and the other indicating the probability of increased activity (i.e., disorders > controls; Fig. 6A, middle). Since some brain regions can show both increased or decreased activity, we generated a combined disease-susceptible map by averaging the two maps and intersecting them with a dataset-specific mask. We performed two analyzes to examine disease susceptibility and DC-$mfSD_{BOLD}$ mismatches. First, we conducted a paired t-test to compare the strength of the DC-$mfSD_{BOLD}$ mismatch (i.e., higher absolute DC residuals) between the brain regions that are susceptible and insusceptible to brain diseases. We further examined whether brain regions that are more susceptible to brain diseases showed higher absolute DC residuals within the disease-susceptible areas. To test this hypothesis, we grouped the disease-susceptibility voxels into five bins according to the ALE score in increments of 0.2 (0:0.2:1) and then averaged the long-range and full-range DC residuals within each bin. We then used repeated-measures ANOVAs to examine whether there were significant main effects of disease susceptibility on absolute DC residuals. Notably, unless otherwise specified, p values were adjusted using the Holm–Bonferroni correction (Holm, 1979) for multiple comparisons.

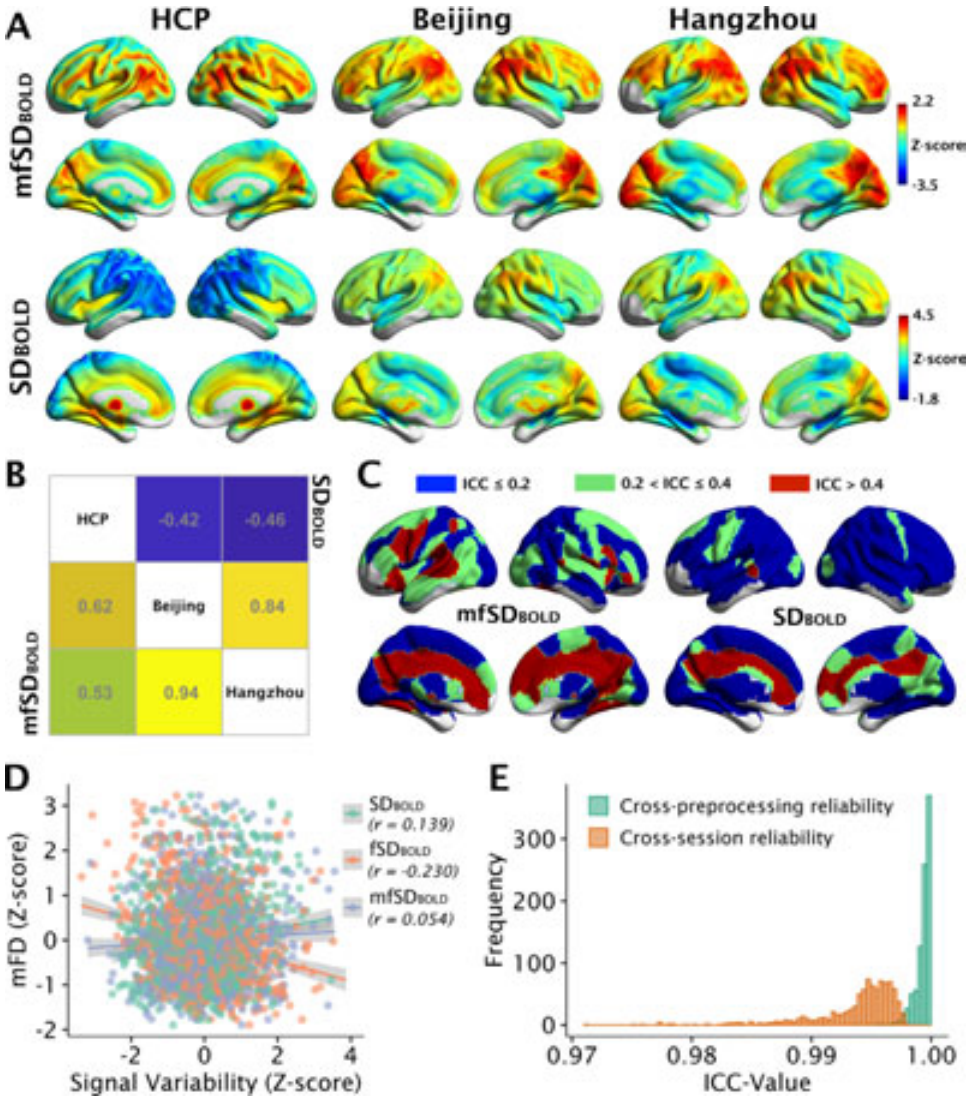

Fig. 1. *Reliability and stability of the signal variability measures.* (A) Group-averaged spatial patterns of $mfSD_{BOLD}$ (upper panel) and SD_{BOLD} (lower panel) for three datasets. (B) Spatial similarity across sites for SD_{BOLD} (upper triangle) and $mfSD_{BOLD}$ (lower triangle) based on the Fan 246 template. (C) Cross-site reliability of $mfSD_{BOLD}$ (left) and SD_{BOLD} (right) for each brain region. (D) Correlations between signal variability and mFD (each dot represents one participant). (E) Reliability of $mfSD_{BOLD}$ cross two sessions (HCP: REST1 and REST2; orange) and different preprocessing parameters (HCP: with and without global signal regression; green) for each individual participant. SD_{BOLD}, standard deviation of the BOLD signal; fSD_{BOLD}, fractional SD_{BOLD}; $mfSD_{BOLD}$, mean-scaled fSD_{BOLD}; ICC, intraclass correlation coefficient; mFD, mean framewise displacement (For interpretation of the references to color in this figure legend, the reader is referred to the web version of this article.).

Results

3.1. $mfSD_{BOLD}$ is a reliable measure of BOLD signal variability

SD_{BOLD} has been used to quantify the variability of the BOLD signal for data from individual scanners. Nevertheless, the intra-site and inter-site reliabilities of BOLD signal variability have not been strictly examined. In particular, the overall signal variability could be affected by the noise level (such as the physiological noise and head motion) and the signal-to-noise ratio of the scanner, making it less reliable across sites. We proposed that the $mfSD_{BOLD}$, which is the mean-scaled proportion of the low-frequency SD_{BOLD} ($0.01 < f < 0.1$ Hz) related to the overall SD_{BOLD} (> 0.01 Hz), could reduce the effect of noise and head motion. We performed several analyzes to validate this measure.

First, we found that $mfSD_{BOLD}$ was highly consistent across datasets (Fig. 1A, upper panel) while SD_{BOLD} was not (Fig. 1A, lower panel). In particular, a high and consistent cross-site correlation was observed for $mfSD_{BOLD}$ ($rs = 0.62, 0.53$ and 0.94, $ps < 10^{-10}$; $ICC = 0.792$) while negative correlations were found between the HCP data and the other two sites ($rs = -0.42$ and -0.46, $ps < 10^{-10}$; $ICC < 0.001$) for SD_{BOLD} (Fig. 1B) based on the Fan 246 template. Direct comparisons revealed higher cross-site pattern similarity for $mfSD_{BOLD}$ than for SD_{BOLD} ($Zs = 12.27, 11.38$ and 5.41, $ps < 10^{-7}$). Similar results were found based on the Yeo 2011 template (Fig. S1A). Notably, although the spatial pattern of $mfSD_{BOLD}$ showed greater cross-scanner consistency than SD_{BOLD}, we found that the spatial pattern similarity of $mfSD_{BOLD}$ between the HCP and Beijing ($r = 0.62$) or Hangzhou ($r = 0.53$) datasets was still lower than that between the Beijing and Hangzhou ($r = 0.94$) datasets (Fig. 1B), which was probably due to the differences in scanner and scanning parameters.

Across different brain regions, we found that $mfSD_{BOLD}$ has high cross-site reliability ($ICC > 0.4$) in the cingulate gyrus, inferior frontal gyrus, inferior parietal lobules and fusiform gyrus (Fig. 1C, left), while SD_{BOLD} has low cross-site reliability ($ICC \leq 0.2$) in many cortical regions except the cingulate gyrus, medial frontal gyrus, and part of the middle temporal gyrus (Fig. 1C, right). In general, the cross-site reliability at different brain regions of $mfSD_{BOLD}$ was higher than that of SD_{BOLD} (paired $t = 12.23$, $p < 0.001$).

Furthermore, we found that the spatial pattern between $mfSD_{BOLD}$ and SD_{BOLD} was quite similar for the Beijing ($r = 0.61 \pm 0.05$; Fig. S1B, left) and Hangzhou ($r = 0.66 \pm 0.08$; Fig. S1B, left) datasets, whereas that for the HCP dataset was much lower ($r = 0.27 \pm 0.06$; Fig. S1B, left). This finding is largely because the spatial pattern of SD_{BOLD} is highly variable across datasets while that for $mfSD_{BOLD}$ is more consistent (Fig. 1B).

Second, a previous study suggested that head motion could affect overall BOLD signal variability (Kublbock et al., 2014). Consistently, using the HCP dataset, we found that SD_{BOLD} ($r = 0.139$, $p < 0.001$)

Table 1
Stability and reliability of BOLD signal variability measures.

		SD_{BOLD}	$mfSD_{BOLD}$
Cross-session reliability	HCP	0.99 ± 0.01	0.99 ± 0.004
(ICC: mean ± sd)	Beijing	No session data	
	Hangzhou		
Cross-site reliability (ICC)	HCP, Beijing, and Hangzhou	0.00	0.79
Robustness to preprocessing	HCP	0.999 ± 0.001	0.999 ± 0.001
parameters	Beijing	0.99 ± 0.01	0.98 ± 0.01
(ICC: mean ± sd)	Hangzhou	0.99 ± 0.01	0.98 ± 0.01
Robustness to head motion	HCP	0.14***	0.05 (n.s.)
(Correlation with mFD, r)	Beijing	0.19***	0.07 (n.s.)
	Hangzhou	-0.2 (n.s.)	0.25 (n.s.)
cross-voxel correlation with CBF (r:	HCP	No CBF data	
mean ± sd)	Beijing		
	Hangzhou	0.39 ± 0.09	0.30 ± 0.09
Cross-voxel correlation with full-range	HCP	0.16 ± 0.07	0.96 ± 0.02
DC (r: mean ± sd)	Beijing	0.45 ± 0.08	0.57 ± 0.06
	Hangzhou	0.46 ± 0.08	0.54 ± 0.09
Cross-voxel correlation with	HCP	-0.20 ± 0.08	0.76 ± 0.02
long-range DC	Beijing	0.33 ± 0.11	0.43 ± 0.08
(r: mean ± sd)	Hangzhou	0.38 ± 0.09	0.42 ± 0.09

Note: The DC correlation threshold of the HCP was 0.1, and that of the Beijing and Hangzhou samples was 0.2; ICC, intra-class correlation coefficient; SD_{BOLD}, standard deviation of BOLD signal; $mfSD_{BOLD}$, mean-scaled fractional standard deviation of BOLD signal; DC, degree centrality; mFD, mean framewise displacement; CBF, cerebral blood flow; HCP, Human Connectome Project. *** $p < 0.001$; *n.s. non-significant.*

and fSD_{BOLD} ($r = -0.230$, $p < 10^{-10}$) were correlated with individuals' head motion (measured by mFD) (Fig. 1D), whereas $mfSD_{BOLD}$ was not ($r = 0.054$, $p = 0.101$) (Fig. 1D). This result was replicated on the Beijing sample (Table 1), which SD_{BOLD} ($r = 0.19$, $p < 0.001$) was affected by head motion, while $mfSD_{BOLD}$ was not ($r = 0.07$, $p = 0.164$). Nevertheless, similar results had not been observed on the Hangzhou sample (Table 1), probably due to the small sample size. It should be noted that mean scaling did not affect the spatial pattern and thus did not affect the cross-site reliability.

Third, both $mfSD_{BOLD}$ (Fig. 1E, orange) and SD_{BOLD} (Table 1) showed remarkably high spatial pattern similarities across sessions from the HCP for each individual (all *ICCs* > 0.90). Finally, the spatial distribution of neither $mfSD_{BOLD}$ (all *ICCs* > 0.90; Fig. 1E, green; Table 1) nor SD_{BOLD} (all *ICCs* > 0.90; Table 1) of each participant in the three datasets was affected by the global signal regression.

As summarized in Table 1, compared to SD_{BOLD}, the spatial pattern of $mfSD_{BOLD}$ was more reliable across sites, although both measures were stable across different sessions and robust to different preprocessing parameters. In addition, the $mfSD_{BOLD}$ was less affected by head movement as compared to SD_{BOLD}. Accordingly, we used $mfSD_{BOLD}$ as the measure of BOLD signal variability in the following primary analyzes.

3.2. Relationships among DC, $mfSD_{BOLD}$ and CBF

To understand the physiological basis of DC and $mfSD_{BOLD}$, we also measured CBF in the Hangzhou sample. Consistent with previous observations (Liang et al., 2013; Sheng et al., 2018), we found a significant positive correlation between DC and CBF at the group level (Fig. 2A; full-range DC & CBF: $rs = 0.480–0.496$ for different thresholds; long-range DC & CBF: $rs = 0.286–0.396$ for different thresholds; $ps_{adj} < 10^{-10}$; $df_{eff} = 993$) based on the mean DC and CBF maps (Fig. S2C), and this positive correlation also occurred for each individual (Fig. 2B; full-range DC & CBF: mean $rs = 0.247–0.279$ for different thresholds; all $ps < 0.01$; $df_{eff} = 993$; long-range DC & CBF: mean $rs = 0.207–0.262$ for different thresholds; all $ps < 0.05$; $df_{eff} = 993$). The correlation with full-range DC was stronger than that with long-range DC (group-level: $Zs = 2.645 \sim 5.088$, $ps_{adj} < 0.01$; individual-level: paired-$ts = 2.089–4.692$; $ps_{adj} < 0.05$).

Intriguingly, $mfSD_{BOLD}$ values were also positively correlated with CBF both at the group level ($r = 0.462$, $p < 10^{-10}$, $df_{eff} = 993$; Fig. 2C) and for each individual (mean $r = 0.296$, *ranging from 0.138 to 0.473*; all $ps < 10^{-5}$, $df_{eff} = 993$; Fig. 2D). The above results suggest that DC and $mfSD_{BOLD}$ share a common physiological basis. Similarly, SD_{BOLD} was also associated with CBF ($r = 0.39 \pm 0.09$, all $ps < 10^{-5}$) (Fig. S3), which is not surprising given that the spatial patterns of SD_{BOLD} and $mfSD_{BOLD}$ for the Hangzhou dataset were remarkably similar (Figs. 1A, S1B).

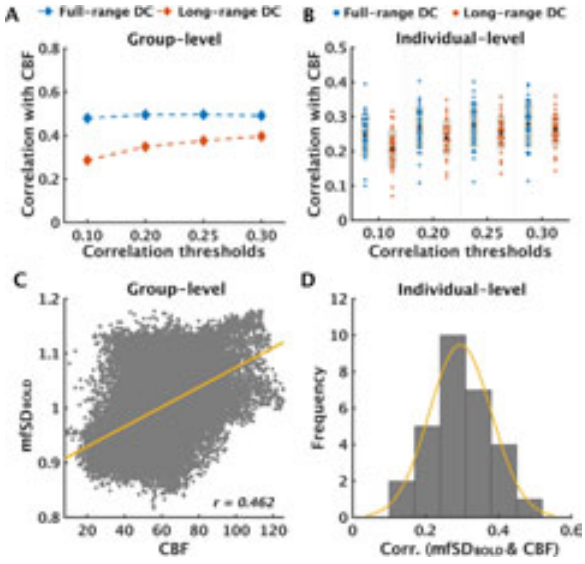

Fig. 2. *Relationships among DC, $mfSD_{BOLD}$ and CBF in the Hangzhou sample.* Correlation between DC and CBF at the (A) group level and (B) individual level under four correlation thresholds of DC calculations. The black dots represent mean correlation coefficients. Each colored dot represents one participant, and the grey areas represent +/- one standard deviation. The correlation between $mfSD_{BOLD}$ and CBF at the (C) group level (each dot represents one voxel in the brain) and (D) individual level. Group-averaged brain maps of DC and CBF; please see Fig. S2C. DC, degree centrality; $mfSD_{BOLD}$, mean-scaled fractional standard deviation of the BOLD signal; CBF, cerebral blood flow; Corr., correlation.

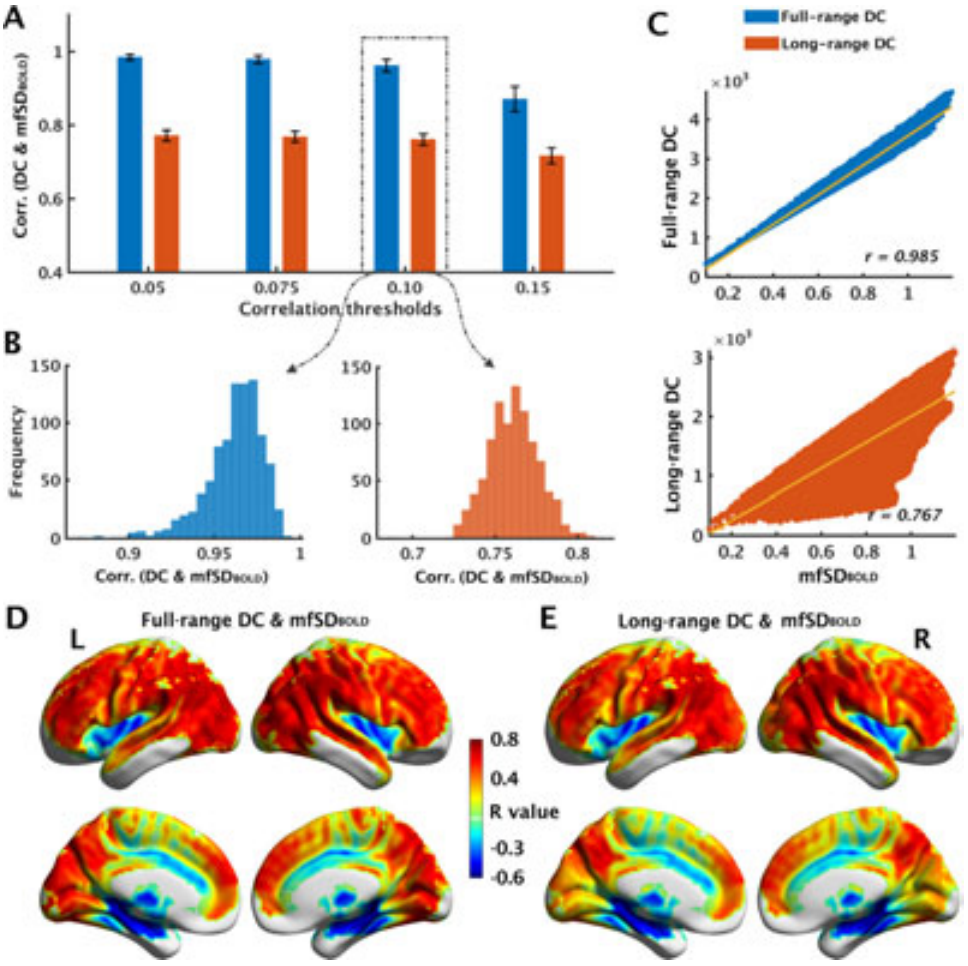

Fig.3. *Correlations between full-range or long-range DC and mfSD$_{BOLD}$.* (A) Cross-voxel correlation between full-range or long-range DC and mfSD$_{BOLD}$ across different correlation thresholds for DC calculations. Error bars represent the standard deviations of the correlation coefficients across participants. (B) Representative histograms of the coupling between mfSD$_{BOLD}$ and full-range (left panel) or long-range DC (right panel) at the individual level. A correlation threshold of 0.10 was used for DC. (C) Scattered distribution of the mfSD$_{BOLD}$ and full-range (upper) or long-range DC (lower) at the group level. A correlation threshold of 0.10 was used for DC. Each dot represents one voxel in the brain. Cross-subject correlations between (D) full-range or (E) long-range DC (correlation threshold of 0.10) and mfSD$_{BOLD}$. The cross-subject results using other DC correlation thresholds were similar and are shown in Fig. S12. For the group-averaged DC maps, please see Fig. S2. DC, degree centrality; mfSD$_{BOLD}$, mean-scaled fractional standard deviation of the BOLD signal; Corr., correlation.

3.3. Tight coupling between DC and mfSD$_{BOLD}$

Having verified the reliability of mfSD$_{BOLD}$ and revealed a common physiological basis of DC and mfSD$_{BOLD}$, we then examined the correlation between DC and mfSD$_{BOLD}$. This correlation was examined across voxels for each participant and across participants for each voxel.

Cross-voxel coupling between DC and mfSD$_{BOLD}$. Consistent with our hypothesis, the Pearson correlation analysis revealed a significantly positive correlation between full-range DC and mfSD$_{BOLD}$ for each participant ($rs = 0.871 \pm 0.034$–0.985 ± 0.008 for different thresholds, $ps_{adj} < 10^{-10}$, $df_{eff} = 3316$) (Fig. 3A & B). After excluding the local connectivity and focusing on long-range DC (Euclidean distance ≥ 75 mm), strong, positive correlations were also observed ($rs = 0.717 \pm 0.022$ –0.772 ± 0.015 for different thresholds, $ps_{adj} < 10^{-10}$, $df_{eff} = 3316$), although the correlation strengths were weaker than those for full-range DC (*paired ts* = 90.008–179.136 for four thresholds, $ps_{adj} < 10^{-10}$) (Fig. 3A & B).

Further validation analyzes found that the cross-voxel couplings between mfSD$_{BOLD}$ and DC were stable across sessions for both full-range DC ($rs = 0.424 \sim 0.479$ for different thresholds, $ps_{adj} < 10^{-10}$, $df = 925$; $ICC = 0.595$–0.647) and long-range DC ($rs = 0.524$–0.656 for different thresholds, $ps_{adj} < 10^{-10}$, $df = 925$; $ICC = 0.688$–0.792) (Fig. S4). Strong cross-voxel couplings were also found for the Beijing and Hangzhou samples that used different scanners (*full-range DC & mfSD$_{BOLD}$*: Beijing: mean $rs = 0.524$–0.599 for different thresholds, $df_{eff} = 1638$; Hangzhou: mean $rs = 0.491$–0.580 for different thresholds, $df_{eff} = 993$; *long-range DC & mfSD$_{BOLD}$*: Beijing: mean $rs = 0.383$–0.465 for different thresholds, $df_{eff} = 1638$; Hangzhou: mean $rs = 0.376$–0.451 for different thresholds, $df_{eff} = 993$) (Fig. S5). The tight cross-voxel couplings between DC and mfSD$_{BOLD}$ were robust regarding the analytic parameter choices, such as network binarization (full-range DC & mfSD$_{BOLD}$: $r > 0.94$ for each individual; long-range DC & mfSD$_{BOLD}$: $r > 0.73$ for each individual) and global signal regression (full-range DC & mfSD$_{BOLD}$: $r > 0.72$ for each individual; long-range DC & mfSD$_{BOLD}$: $r > 0.66$ for each individual) (Fig. S6).

Positive couplings were found for each single participant, although the degrees varied across participants (Fig. 3A & B). Across different correlation thresholds for DC calculations, the individual differences in DC-mfSD$_{BOLD}$ coupling were quite consistent (Fig. S7; full-range DC & mfSD$_{BOLD}$: $ICC = 0.92$; long-range DC & mfSD$_{BOLD}$: $ICC = 0.95$).

However, when examining the correlation between SD$_{BOLD}$ and DC (cut-off threshold equals 0.10 and 0.20 for the HCP and Beijing/Hangzhou datasets, respectively), we did not find consistent positive correlations between SD$_{BOLD}$ and full-range DC (HCP: $r = 0.16 \pm 0.07$; Beijing: $r = 0.45 \pm 0.08$; Hangzhou: $r = 0.46 \pm 0.08$) or long-range DC (HCP: $r = -0.20 \pm 0.08$; Beijing: $r = 0.33 \pm 0.11$; Hangzhou: $r = 0.38 \pm 0.09$) (Table 1; Fig. S8).

Cross-subject coupling between DC and mfSD$_{BOLD}$. Having shown the significant cross-voxel coupling between DC and mfSD$_{BOLD}$, we further examined whether there was significant cross-subject coupling, i.e., whether participants showing greater DC also exhibited greater mfSD$_{BOLD}$. Indeed, we found strong and positive cross-subject couplings in most brain regions for both full-range (Fig. 3D) and long-range DC (Fig. 3E). The strongest positive full/long-range DC-mfSD$_{BOLD}$ couplings ($r > 0.65$) were found in the bilateral frontal, occipital, and parietal lobe regions (Table S2). Interestingly, we also found some negative correlations between full/long-range DC and mfSD$_{BOLD}$ correlations, with the strongest negative correlations ($r < -0.55$) located in the left an-

Table 2
Effects of age and sex on the cognitive total composite scores and DC-mfSD$_{BOLD}$ couplings.

Dependent variables		Term	Statistic	*P*.value	P.adj
CogTotalComp		**Age**	**-2.813**	**0.005**	**0.015**
		Sex (males)	-1.252	0.211	0.211
		Age:Sex	1.622	0.105	0.21
R = 0.05	Full-range DC & mfSDBOLD	**Age**	**3.284**	**0.001**	**0.006**
		Sex (males)	0.466	0.641	1
		Age:Sex	-0.265	0.791	0.791
	Long-range DC & mfSDBOLD	**Age**	**-3.094**	**0.002**	**0.010**
		Sex (males)	1.687	0.092	0.368
		Age:Sex	-1.108	0.268	0.804
R = 0.075	Full-range DC & mfSDBOLD	Age	1.697	0.09	0.360
		Sex (males)	0.226	0.821	1
		Age:Sex	0.206	0.837	0.837
	Long-range DC & mfSDBOLD	**Age**	**-3.145**	**0.002**	**0.012**
		Sex (males)	1.762	0.078	0.390
		Age:Sex	-1.146	0.252	0.756
R = 0.10	Full-range DC & mfSDBOLD	Age	0.225	0.822	1
		Sex (males)	-0.035	0.972	0.972
		Age:Sex	0.646	0.518	1
	Long-range DC & mfSDBOLD	**Age**	**-3.206**	**0.001**	**0.006**
		Sex (males)	1.778	0.076	0.380
		Age:Sex	-1.072	0.284	1
R = 0.15	Full-range DC & mfSDBOLD	Age	-1.641	0.101	0.505
		Sex (males)	-0.122	0.903	0.903
		Age:Sex	0.899	0.369	1
	Long-range DC & mfSDBOLD	**Age**	**-2.936**	**0.003**	**0.018**
		Sex (males)	1.343	0.18	0.720
		Age:Sex	-0.458	0.647	1

Note: CogTotalComp, cognitive total composite scores; DC, degree centrality; mfSD$_{BOLD}$, mean-scaled fractional standard deviation of the BOLD signal.

terior cerebellum lobe, bilateral hippocampus, and left putamen (Table S3). In an analysis of 356 unrelated participants, the results were also stable (Fig. S9). Again, the spatial pattern of cross-subject coupling was quite reliable across sessions (Fig. S10; all *ICCs* $\geq$ *0.97*), analytic parameters (Fig. S11; all *ICCs* $\geq$ *0.93*), and correlation thresholds for DC calculations (Fig. S12; *ICC* $\geq$ *0.99*). Given the small sample size of the Hangzhou dataset (N = 29), the reliability of the cross-subject DC-mfSD$_{BOLD}$ correlation was measured by calculating the pattern similarity of the uncorrected correlation brain maps between the HCP (N = 927) and Beijing (N = 416; Fig. S13A) datasets. The cross-subject correlation between full-range DC and mfSD$_{BOLD}$ was less reliable (Fig. S13B; Left: full-range DC & mfSD$_{BOLD}$: *ICC = 0.22;* long-range DC & mfSD$_{BOLD}$: *ICC = 0.36*; Right: full-range DC & mfSD$_{BOLD}$: *ICC = 0.00;* long-range DC & mfSD$_{BOLD}$: *ICC = 0.29*).

3.4. Functional relevance of DC-mfSD$_{BOLD}$ coupling

The above analyzes revealed tight cross-voxel and cross-subject couplings between DC and mfSD$_{BOLD}$. In addition to the overall strong coupling, we also found significant differences in coupling strength across participants and brain voxels. If DC-mfSD$_{BOLD}$ coupling reflects a fundamental organizing principle of the human brain, deviation from this coupling should have functional consequences. In particular, we predicted that participants with stronger coupling would show better cognitive performance and brain regions deviating from this coupling would be more susceptible to malfunctions. We performed several analyzes to test these intriguing hypotheses using the HCP dataset.

3.4.1. Coupling strength related to individual cognitive performance

Two analyzes were performed to examine the relationship between individual coupling strength and cognitive performance. In the first analysis, we examined the effects of age and sex on cognitive performance and DC-mfSD$_{BOLD}$ coupling strength through linear least-square regression models. We found that the cognitive total composite scores significantly decreased with age (*t = -2.81, p = 0.005*; Table 2). The main effect of sex and the interaction between age and sex on the cognitive total composite scores were not significant (Table 2; *ps > 0.05*). In parallel, we also found that the coupling between long-range DC and mfSD$_{BOLD}$ significantly decreased with age (*ts* $\geq$ *-2.94, ps$_{adj}$ < 0.05*; Table 2), although the age effect was not consistent for full-range DC-mfSD$_{BOLD}$ coupling across different cut-off thresholds (Table 2). Additionally, the main effects of sex and age by sex interaction were not significant (Table 2; all *ps > 0.05*). Consistent results were found when only unrelated participants were used (Table S4).

In the second analysis, we further examined whether the strength of DC-mfSD$_{BOLD}$ coupling and cognitive performance was correlated across participants after controlling for age, sex, age^2, age $\times$ sex, age^2 $\times$ sex and mFD. We found that the coupling strength between long-range DC and mfSD$_{BOLD}$ was positively correlated with the cognitive total composite scores across four correlation thresholds for DC (*rs = 0.09 ~ 0.11, ps$_{adj}$ < 0.05*; Fig. 4A; Table 3). No significant correlation was found for the coupling strength of full-range DC and mfSD$_{BOLD}$ (*rs = 0.02 ~ 0.04, ps$_{unadj}$ > 0.05*; Fig. 4A; Table 3). We also found comparable correlation coefficients when using unrelated participants (CogTotalComp & full-range DC-mfSD$_{BOLD}$: *rs = 0.07–0.08, ps$_{unadj}$ > 0.05*; CogTotalComp & long-range DC-mfSD$_{BOLD}$: *rs = 0.09–0.11, ps$_{unadj}$ = 0.017–0.032*), although the statistical significance was lower due to the reduced sample size. However, the coupling of DC (correlation threshold = 0.1) and SD$_{BOLD}$ was not associated with cognitive performance (CogTotalComp & full-range DC-SD$_{BOLD}$: *r = -0.004, p = 0.909*; CogTotalComp & long-range DC-mfSD$_{BOLD}$: *r = -0.006, p = 0.848*; Table 3).

Previous studies have implicated short-range connections (ranging from 20 mm to 75 mm) in functional segregation in the human cortex (Duan et al., 2019; Sporns, 2013). We also examined the cross-voxel coupling of short-range DC (correlation threshold = 0.1) and mfSD$_{BOLD}$ and their functional relevance based on the HCP dataset. We found that although short-range DC was also positively correlated with mfSD$_{BOLD}$ (*rs = 0.686 ± 0.017, ps < 0.001*) for all participants, the degree of coupling did not correlate with cognition (*r = 0.001, p = 0.973*), suggesting the specific functional role of long-range DC and mfSD$_{BOLD}$ coupling. Across participants, we did not find any brain region where the DC, mfSD$_{BOLD}$ or SD$_{BOLD}$ values were significantly correlated with cognitive performance.

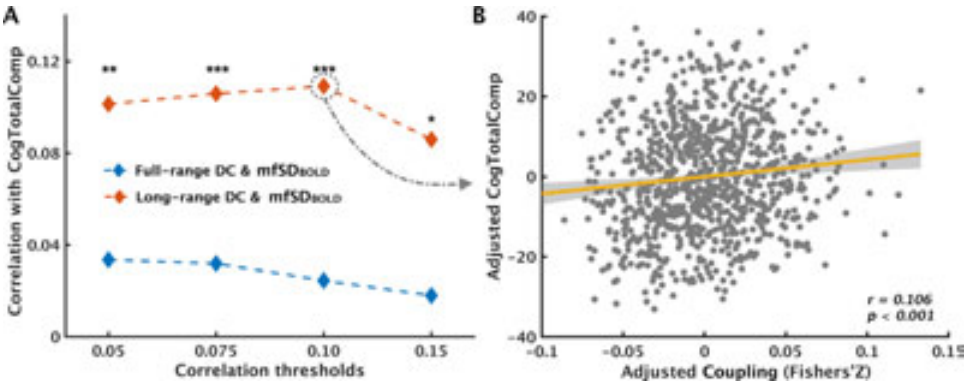

Fig. 4. *Coupling strength is associated with individual cognitive performance.* (A) Relationships between the coupling of DC and $mfSD_{BOLD}$ with cognitive total composite scores evaluated separately for each DC threshold. (B) Scatter plot of the strength of long-range DC (with a threshold of 0.10) and $mfSD_{BOLD}$ coupling and the cognitive total composite scores after controlling for confounding variables (each dot represents one participant). CogTotalComp, cognitive total composite scores; DC, degree centrality; $mfSD_{BOLD}$, mean-scaled fractional standard deviation of the BOLD signal. * $p_{adj} < 0.05$, ** $p_{adj} < 0.01$, *** $p_{adj} < 0.001$.

Table 3
Relationships between cross-voxel coupling of DC and signal variability (SD_{BOLD} vs $mfSD_{BOLD}$) and cognitive performance for the HCP data.

		SD_{BOLD}	$mfSD_{BOLD}$
The strength of cross-voxel coupling and cognition	Full-range DC	-0.004 (*n.s.*)	0.03 (*n.s.*)
	Long-range DC	-0.006 (*n.s.*)	***0.11******
The residual of cross-voxel coupling and cognition	Full-range DC	-	-
	Long-range DC	-	**rSTG** (*r* = *-0.197****)
			rMCC (r = -0.198***)

Note: The correlation threshold of DC was 0.1. SD_{BOLD}, standard deviation of BOLD signal; $mfSD_{BOLD}$, mean-scaled fractional standard deviation of BOLD signal; DC, degree centrality; rSTG, right superior temporal gyrus; rMCC, right middle cingulate cortex. *** $p_{adj} < 0.001$; *n.s. non-significant; - no statistically significant brain region.*

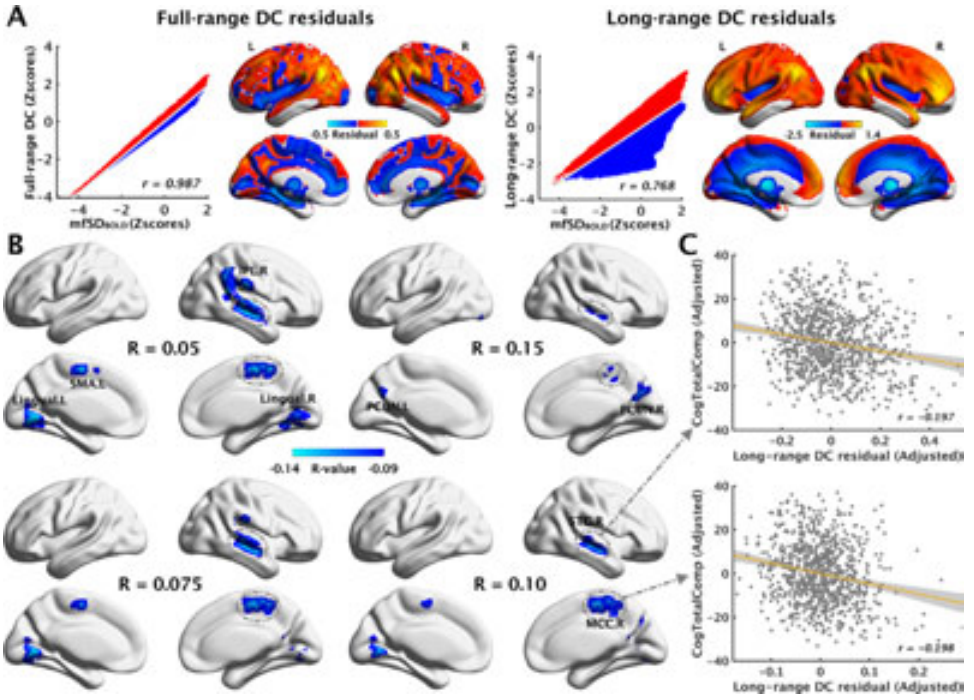

Fig. 5. *Relationships between long-range DC residuals and cognitive total composite scores.* (A) Brain maps of full/long-range DC residuals (based on group-average DC and $mfSD_{BOLD}$ maps). Red (yellow), overloading (DC > $mfSD_{BOLD}$); blue, underloading (DC < $mfSD_{BOLD}$). (B) Absolute long-range DC residuals of the right STG and right MCC were significantly and negatively correlated with cognitive total composite scores under four different thresholds of DC after regressing out confounding variables (age, sex, age^2, age × sex interaction, age^2 × sex interaction and mFD). (C) Scatter plots of negative correlations between absolute long-range DC residuals and cognitive total composite scores (each dot represents one participant). DC, degree centrality; CogTotalComp, cognitive total composite scores; mFD, mean framewise displacement; STG, superior temporal gyrus; MCC, middle cingulate cortex; IPL, inferior parietal lobule; SMA, supplementary motor area; PCUN, precuneus; R, right; L, left (For interpretation of the references to color in this figure legend, the reader is referred to the web version of this article.).

3.4.2. Residuals of DC-$mfSD_{BOLD}$ coupling related to cognitive performance

In addition to the overall coupling strength, we further examined the regional differences in DC-$mfSD_{BOLD}$ coupling and their relationships to brain functions. In the cross-voxel analysis, we constructed least-squares linear regression models for DC and $mfSD_{BOLD}$. The regional mismatches between DC and $mfSD_{BOLD}$ were defined as the residual DC after regressing out $mfSD_{BOLD}$ (Fig. 5A). We found that DC residuals were very stable and reliable across sessions (Fig. S14A; full-range DC residuals: mean *ICC* = *0.568–0.808* for different thresholds; long-range DC residuals: mean *ICC* = *0.949–0.987* for different thresholds), datasets (Fig. S14B; full-range DC residuals: *rs* = *0.184, 0.347* and *0.812, ICC* = *0.724*; long-range DC residuals: *rs* = *0.769, 0.742* and *0.963, ICC* = *0.928*), and thresholds (Fig. S14C; full-range DC residual: *ICC* = *0.842*; long-range DC residual: *ICC* = *0.992*). Overall, the reliability was higher for long-range DC residuals than for full-range DC residuals (Fig. S14).

We then examined whether the mismatch between DC and $mfSD_{BOLD}$ was related to individual cognitive performance. To address this question, we performed partial correlation analyzes for full-range/long-range DC residuals and cognitive function composite scores after controlling for age, sex, age^2, age × sex interaction, age^2 × sex interac-

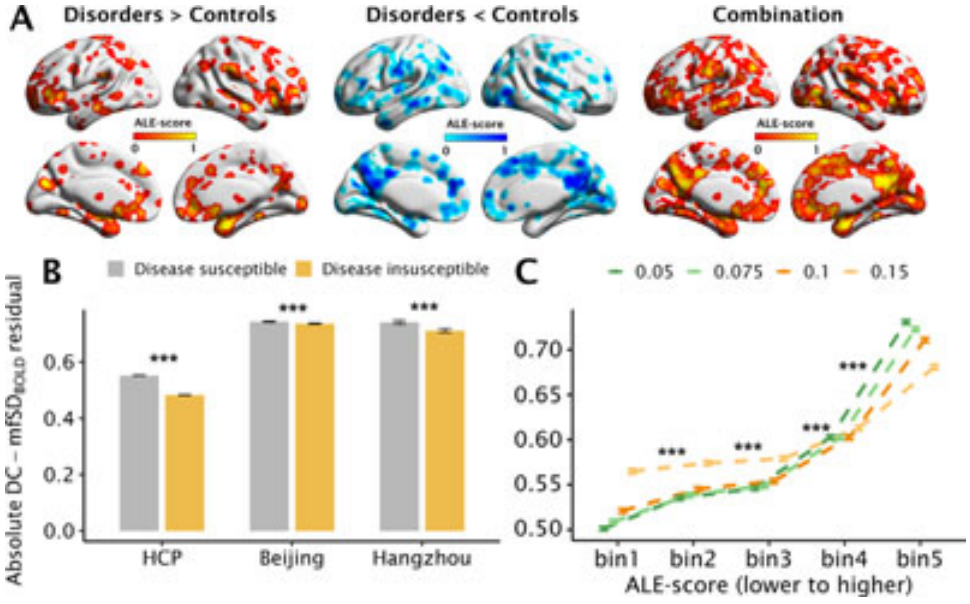

Fig. 6. *Brain regions showing mismatches between long-range DC and mfSD$_{BOLD}$ were susceptible to brain diseases.* (A) Susceptible maps of brain diseases from Sha et al. (2018). The ALE maps of higher (left) and lower (middle) disease-associated activities were averaged to generate the common disease-susceptible map (right). (B) Absolute long-range DC residuals were higher in regions that are susceptible to diseases than in regions that are not susceptible to the HCP (correlation threshold of DC = 0.1), Beijing and Hangzhou (DC correlation threshold of DC = 0.2) datasets. Error bars represent within-subject standard errors. (C) Absolute long-range DC residuals in brain regions show different degrees of disease susceptibility for the HCP dataset. The brain susceptibility regions were divided into 5 bins based on susceptibility (i.e., ALE score). Error bars represent 99% confidence interval within-subject standard errors. *** $p_{adj} < 0.001$.

tion and mFD. We found that the absolute long-range DC residuals in the right superior temporal gyrus (STG) and right middle cingulate cortex (MCC) (Fig. 5B & C) were significantly and negatively correlated with cognitive performance under four different thresholds of DC. None of the brain regions showed a significant correlation between absolute full-range DC residuals and cognitive performance. When the same analyzes were performed on unrelated participants from the HCP dataset (N = 356), we also found a negative correlation between the absolute long-range DC residuals and cognitive performance in the right MCC and right STG (Fig. S15) across four thresholds of DC, although the correlations were not statistically significant after multiple comparison corrections. In contrast, we did not find any brain region where the residuals of DC-SD$_{BOLD}$ coupling were significantly correlated with cognitive performance (Table 3).

To further examine whether the direction of mismatches affects cognitive performance, we used the raw residual instead of the absolute residual. We found that the right STG (Fig. S16A, left panel) showed positive long-range DC residuals (Fig. S16A, middle panel), which were significantly *negatively* correlated with cognitive performance (Fig. S16A, right panel). In contrast, the right MCC (Fig. S16B, left panel) showed overall negative long-range DC residuals (Fig. S16B, middle panel), which were significantly *positively* correlated with cognitive performance (Fig. S16B, right panel). The results together suggest that participants with greater deviation (positive or negative) from the long-range DC-mfSD$_{BOLD}$ coupling showed worse cognitive function.

3.4.3. Mismatched brain regions are susceptible to brain diseases

The above analyzes suggest that a greater mismatch in mfSD$_{BOLD}$ and DC was related to worse cognitive permanence. A further question follows: were the regions showing a greater mismatch also more vulnerable to brain diseases? To answer this question, we defined the disease-susceptible areas (for details, please see *Materials and Methods*) from the results of a meta-analysis (Sha et al., 2018) and conducted a paired *t*-test to explore whether the strength of the DC-mfSD$_{BOLD}$ mismatches of the disease-susceptible areas is significantly higher than that of insusceptible regions. The results revealed that for HCP sample, the absolute DC residuals within the disease-susceptible regions (number of voxels = 40323) were significantly larger than those outside of the disease-susceptible regions (number of voxels = 65878) for both long-range DC residuals (*paired-ts = 137.278–207.098* for different thresholds, $ps_{adj} < 10^{-10}$) (Fig. 6B; Table 4) and full-range DC residuals (*paired-ts = 33.480–70.838* for different thresholds; $ps_{adj} < 10^{-10}$) (Table 4).

Table 4
The differences in DC and signal variability (SD$_{BOLD}$ vs mfSD$_{BOLD}$) residuals between disease susceptible and insusceptible brain regions.

		SD$_{BOLD}$ (Susceptible - Insusceptible: *paired-t*)	**mfSD$_{BOLD}$**
Full-range DC residual	HCP	**-110.32*****	**47.21*****
	Beijing	**-12.17*****	**-11.66*****
	Hangzhou	-1.46 (*n.s.*)	1.55 (*n.s.*)
Long-range DC residual	HCP	**-141.06*****	**166.85*****
	Beijing	**5.86*****	**4.85*****
	Hangzhou	1.24 (*n.s.*)	**5.95*****

Note: The DC correlation threshold of the HCP was 0.1, and that of the Beijing and Hangzhou samples was 0.2; SD$_{BOLD}$, standard deviation of BOLD signal; mfSD$_{BOLD}$, mean-scaled fractional standard deviation of BOLD signal; DC, degree centrality; HCP, Human Connectome Project. *** $p_{adj} < 0.001$; *n.s. non-significant.*

Using the Beijing and Hangzhou datasets, we also found the absolute long-range DC (correlation threshold = 0.2) residuals within the disease-susceptible regions (Beijing: number of voxels = 12279; Hangzhou: number of voxels = 13829) were significantly larger (Beijing: *paired-t = 4.85, p < 0.001*; Hangzhou: *paired-t = 5.95, p < 0.001*) than those outside of the disease-susceptible regions (Beijing: number of voxels = 24086; Hangzhou: number of voxels = 27219) (Table 4; Fig. 6B), but the absolute full-range DC residuals were smaller within the disease-susceptible regions than those outside of the disease-susceptible regions for the Beijing dataset (*paired-t = -11.66, p < 0.001),* and no difference was found for the Hangzhou dataset (*paired-t = 1.55, p = 0.132*) (Table 4). These results suggest that the long-range DC and mfSD$_{BOLD}$ coupling is a more reliable indicator of brain function, consistent with the finding on the strength of coupling and cognitive performance.

We further examined whether DC-SD$_{BOLD}$ mismatches were also related to disease susceptibilities. The results showed that, for full-range DC, the residuals in the disease-susceptible area were smaller than those outside the disease-susceptible area for the HCP (*paired-t = -110.32, p < 0.001*) and Beijing (*paired-t = -12.17, p < 0.001*) datasets, but not for the Hangzhou dataset (*paired-t = -1.46, p = 0.156*) (Table 4; Fig. S17A). For long-range DC, compared to the residuals outside the disease-susceptible regions, those within the disease-susceptible regions were smaller for the HCP dataset (*paired-t = -141.06, p < 0.001*), greater for the Beijing

dataset (*paired-t = 5.86, p < 0.001*), and not different for the Hangzhou dataset (*paired-t = 1.24, p = 0.225*) (Table 4; Fig. S17B).

In a further analysis, we examined whether the more susceptible brain regions showed higher DC-mfSD$_{BOLD}$ mismatches within the disease-susceptible areas. To test this hypothesis, we grouped the disease susceptibility voxels into five bins according to the ALE score in steps of 0.2 (0:0.2:1) and then averaged the long-range and full-range DC residuals within each bin. A repeated-measures ANOVA revealed a significant main effect of disease susceptibility on long-range DC-mfSD$_{BOLD}$ residuals at all correlation thresholds for the HCP dataset ($F = 4435.9 \sim 56439$, $ps < 10^{-10}$) (Fig. 6C and also see Table S5 for details of the post hoc tests). However, no such relationship was found for the Beijing and Hangzhou datasets or for the full-range DC-mfSD$_{BOLD}$ residuals. These results further suggest that brain regions deviating from long-range DC-mfSD$_{BOLD}$ coupling are more susceptible to mental diseases.

Discussion

In the current study, we examined how the coupling between BOLD signal variability and degree centrality is related to brain functions. We found strong and reproducible coupling between BOLD signal variability and degree centrality across sessions and scanning sites. Furthermore, the strength of coupling was related to cognitive functions, and the regions with decoupling were susceptible to brain diseases. Altogether, these findings reveal an important balance of brain signal variability and informative integration, which is essential for brain functions.

4.1. mfSD$_{BOLD}$ was stable and reliable

The first goal of the current study was to validate a BOLD signal variability measure that would be reliable across datasets and sessions and less affected by head motion artefacts. We found that the traditional BOLD signal variation measure, i.e., SD$_{BOLD}$, showed quite different or even opposite spatial patterns across different datasets. For example, relatively stronger SD$_{BOLD}$ values were found in the thalamus, hippocampus, and anterior cingulate cortex in the HCP dataset, while weaker SD$_{BOLD}$ values were found in these structures than other regions in the Beijing and Hangzhou datasets. A change in BOLD contrast could be described as a change in the transverse relaxation rate or R_2^* (the inverse of T_2^*) due to changes in blood oxygenation (Bandettini et al., 1994; Menon et al., 1993; Ogawa et al., 1990), although it was also related to S_0 (when TE = 0) (Kundu et al., 2012) and TE (Bandettini et al., 1994; Evans et al., 2015). In the single-echo fMRI data, whether the change is due to a changed decay rate or a changed starting intensity cannot be determined. Therefore, it has been difficult to remove the influence of these effects (Birn et al., 2006; Power et al., 2015), even when performing bandpass filtering. Importantly, by calculating the ratio of low-frequency signal fluctuations to full-frequency signal fluctuations, we could effectively suppress these effects on BOLD signal variability and generate a more reliable spatial pattern across sites, which is consistent with a previous study that measured BOLD variability with ALFF (Zou et al., 2008). It should be noted that multi-echo fMRI could also control S_0 and TE to minimize the influence of these unrelated variables (Evans et al., 2015; Kundu et al., 2012).

In addition, we demonstrated that the mean fSD$_{BOLD}$ of grey matter is correlated with head motion across subjects, which may be partially related to the introduction of a strong high-frequency signal with head movement. Since the fSD$_{BOLD}$ reflected the ratio of the low-frequency signal variation to the variation in the overall signal (> 0.01 Hz), it was negatively correlated with head motion. A previous study based on fALFF found similar results (Satterthwaite et al., 2012). Since the effect of head motion on neural signals is global, a normalization process, i.e., division by the mean fSD$_{BOLD}$ of the whole brain, could retain the spatial patterns but reduce the effect of head motion on overall signal variability (Kublbock et al., 2014; Zou et al., 2008). Finally, we found that the mfSD$_{BOLD}$ showed remarkably high reliability and was unaffected by global signal regression. All these characteristics suggest that the mfSD$_{BOLD}$ could be an ideal index for future studies to examine BOLD signal variability.

4.2. Tight coupling between mfSD$_{BOLD}$ and DC

The current study revealed a consistent and robust coupling between DC and mfSD$_{BOLD}$ in all three datasets, both cross-voxels and cross-subjects. The reliability of this coupling was further proven by its robustness to processing parameters. The tight coupling was also consistent with previous studies that used different indicators of brain signal variability, such as f/ALFF (Di et al., 2013; Sato et al., 2019; Tomasi et al., 2016; Yan et al., 2017), sample entropy (Misic et al., 2011), and SD$_{BOLD}$ (Garrett et al., 2018). Although f/SD$_{BOLD}$ and f/ALFF have been separately used in previous studies, our data suggest that they are strongly associated ($r > 0.9$) (Fig. S18). Compared to ALFF (Zang et al., 2007), SD$_{BOLD}$ may be easier to calculate and better to understand (Garrett et al., 2010; Kannurpatti and Biswal, 2008). Unlike ALFF, SD$_{BOLD}$ can be easily applied to time-discontinuous fMRI data, such as data using blocked design, since frequencies estimated from discontinuous, concatenated data could be contaminated by the block boundaries.

Sample entropy, on the other hand, is generally used as a measure of signal complexity, although it is sometimes also used to describe signal variability. Given the different theorization between the sample entropy and the SD$_{BOLD}$, these two indices might capture different aspects of signal variability. For example, sample entropy and SD$_{BOLD}$ measured by BOLD fMRI showed a significant anti-correlation (Shafiei et al., 2019). Moreover, mixed results have been found regarding the relationship between entropy and FC (McDonough and Nashiro, 2014a; Liu et al., 2019; ; McIntosh et al., 2014; Misic et al., 2011; Shafiei et al., 2019). For example, an EEG study separately examined short-range/high frequency (i.e., fine scale) temporal variability and long-range/low-frequency (i.e., coarse scale) temporal variability and revealed positive correlations between entropy and DC at both time scales (Misic et al., 2011). A study using fMRI, however, revealed a negative association between entropy and FC at fine scales but a positive association at coarse scales (McDonough and Nashiro, 2014a). Another fMRI study observed a weak and negative relationship between increased entropy and decreased FC as a result of dopamine depletion via acute phenylalanine/tyrosine depletion (Shafiei et al., 2019). Therefore, whether SD or sample entropy captures different aspects of brain information processing at different timescales and different brain regions remains to be examined. Future studies integrating and comparing these measures will yield more insights into brain dynamics and their functions.

Notably, the cross-voxel correlations between mfSD$_{BOLD}$ and DC were positive for all participants, but the cross-subject correlations were negative for some brain regions in the HCP dataset. The brain regions showing negative correlations were mainly located in subcortical regions (such as the hippocampus, amygdala, putamen, thalamus, etc.) and the cerebellum, which exhibited worse temporal signal-to-noise ratios than cortical regions (Autio et al., 2020). Furthermore, we were unable to replicate the negative correlations in the Beijing dataset with a large sample ($N = 416$). Future studies should examine the reliability of this negative correlation.

Finally, both mfSD$_{BOLD}$ and FC were correlated with regional CBF. This result replicates and extends previous studies showing a close relationship between regional CBF and FC (Liang et al., 2013; Sheng et al., 2018; Tomasi et al., 2013). Our results further indicate that FC and signal variability might have a common physiological basis (Tomasi and Volkow, 2018). Given the relatively consistent pattern cross-scanner for mfSD$_{BOLD}$, we predict that this correlation between mfSD$_{BOLD}$ and CBF could hold across scanners, although empirical data are required to verify this prediction. Together, these findings provide clear and strong evidence to support the robust coupling between DC and mfSD$_{BOLD}$.

4.3. Functional relevance of DC-mfSD$_{BOLD}$ coupling

The strong coupling between signal variability and functional integration within-subjects might reflect a synergy in nodal function and its network role in information processing. On the one hand, extant studies suggest that brain signal variability may represent a potentially meaningful and stable property of the human brain (Zuo et al., 2010), which reflects neural dynamic range or flexibility (Garrett et al., 2014; Garrett et al., 2013b; Nomi et al., 2017) and the capability of information processing (Wang et al., 2018). Increased SD$_{BOLD}$ has been found for younger adults compared to elderly adults (Garrett et al., 2010, 2013a, 2017). Furthermore, SD$_{BOLD}$ increases from rest to task and increases with task difficulty (Garrett et al., 2014). Studies have also reported reduced regional variability in a variety of brain diseases, such as stroke (Kielar et al., 2016), Alzheimer's disease (Scarapicchia et al., 2018), multiple sclerosis (Petracca et al., 2017), and other neurological disorders (Zoller et al., 2017). Dopamine can boost SD$_{BOLD}$, thereby improving individuals' cognitive performance (Garrett et al., 2015; Guitart-Masip et al., 2016).

On the other hand, the DC of a node refers to the number of edges attached to the node (Buckner et al., 2009), which quantifies the communication between brain regions required to exchange information. A larger DC of a brain area may indicate its greater role in information processing. Collectively, these findings suggest that the human brain as a self-organizing system could achieve a high level of matching capability and responsibility.

To test these ideas, we directly examined the functional relevance of the coupling for the first time. We found that the strength of DC-mfSD$_{BOLD}$ coupling was associated with cognitive function, while deviation from this coupling was related to worse cognitive functions and higher susceptibility to brain diseases. First, we found that the strength of mfSD$_{BOLD}$ and long-range DC coupling decreased with increasing age, which was accompanied by decreased cognitive performance. Similarly, Yan et al. (2017) found that the concordance among f/ALFF, DC and regional homogeneity was negatively correlated with age (range from 8 to 86 years old). Second, the degree of mfSD$_{BOLD}$ and long-range DC coupling was significantly related to individuals' comprehensive cognitive performance, even after controlling for age and sex. Third, the greater mismatches between long-range DC and mfSD$_{BOLD}$ in the right STG and MCC were associated with worse comprehensive cognitive performance. Finally, the brain regions with DC-mfSD$_{BOLD}$ mismatches were vulnerable to brain disorders. Together, these results suggest that the synergy of functional integration and brain signal variability plays an important role in the well-functioning brains of individuals.

In addition, we found that the coupling between the mfSD$_{BOLD}$ and full-range DC is stronger than that with long-range DC, but the coupling strength of the mfSD$_{BOLD}$ and long-range DC is more reliable and is strongly and reliably predictive of cognitive functions and susceptibility to brain diseases. It should be noted that the contribution of ultrashort connections (Euclidean distance < 20 mm) to full-range DC was excluded to reduce noise (Power et al., 2012, 2011). These results suggest that long-range DC might be more relevant to higher-level brain functions while short-range connections (20 mm ≤ Euclidean distance < 75 mm) present limited relevance for comprehensive cognitive ability. In particular, long-range connections could provide quick links to other brain regions in the network (Achard et al., 2006) and integrate information between segregated modules (He et al., 2009), thus enabling efficient information processing. As such, the coupling between long-range DC and mfSD$_{BOLD}$ is more critical to achieve optimal brain functions than full-range DC and mfSD$_{BOLD}$ coupling.

4.4. Implications and future directions

The strong coupling between signal variability and FC and its correlation with brain functions provides a new perspective to improve the present understanding of how the brain works. A functioning brain requires good synergy between node capability and responsibility in network information integration. Several lines of future studies could be fruitful. First, the current study revealed a small yet significant age effect on the strength of long-range DC and mfSD$_{BOLD}$ coupling in our sample with a narrow age span. A previous study found weak and heterogeneous coupling between DC and SD$_{BOLD}$ in children and young adolescents, with correlation coefficients varying from -0.2 to 0.5 (Sato et al., 2019), and these findings were most likely due to the age effect. Future studies can expand the age range to examine life span changes in this coupling, which could improve the present understanding of the developmental changes in brain functions. Second, our findings suggest that the coupling between BOLD signal variability and degree centrality is robust, reliable, and functionally significant, which raises the question regarding the biological meaning of this coupling. Although a systematic examination of this important question is certainly beyond the scope of this study, we did find that both mfSD$_{BOLD}$ and DC were related to CBF, indicating that the coupling of mfSD$_{BOLD}$ and DC might share a common metabolic basis. Future studies along this direction could lead to a more mechanistic understanding of this coupling. Third, future studies should examine DC-mfSD$_{BOLD}$ coupling between healthy individuals and patients with brain diseases and examine the link between the degree of mismatches and the severity of brain diseases, which could improve our understanding of brain functional abnormalities and identify targets for intervention. Fourth, although our results indicate that the mismatch between mfSD$_{BOLD}$ and DC has functional consequences, precisely what could contribute to the mismatch and the neural mechanisms underlying the association between the mismatch and brain function still require further study. Finally, future studies could use pharmacological manipulation or noninvasive brain stimulations to examine the causal relationship between functional integration and signal variability, which could contribute to the understanding of the origins of the coupling.

Conclusions

To summarize, our findings suggest that the human brain, as a complex functional system, exhibits strong coupling between regional signal variability and functional integration (as measured by both full-range and long-range DC). Furthermore, the greater coupling is predictive of higher cognitive ability, and the higher decoupling is associated with worse brain function and susceptibility to brain diseases. Our study not only provides a novel brain marker for brain functions but also provides a new perspective on how the brain is organized to achieve efficient information transformation and integration.

Declaration of Competing Interest

The authors declare no conflict of interest.

Credit authorship contribution statement

Jintao Sheng: Conceptualization, Methodology, Software, Formal analysis, Visualization, Data curation, Writing - original draft. **Liang Zhang:** Investigation, Methodology. **Junjiao Feng:** Investigation. **Jing Liu:** Investigation. **Anqi Li:** Investigation. **Wei Chen:** Resources. **Yuedi Shen:** Resources. **Jinhui Wang:** Writing – review & editing. **Gui Xue:** Conceptualization, Data curation, Funding acquisition, Investigation, Methodology, Project administration, Resources, Supervision, Validation, Writing - review & editing.

Acknowledgment

This work was sponsored by the National Natural Science Foundation of China (31730038), the NSFC and the Israel Science Foundation (ISF) joint project (31861143040), the Sino-German Collaborative Research Project "Crossmodal Learning" (NSFC 62061136001/DFG TRR169), and the Guangdong Pearl River Talents Plan Innovative and Entrepreneurial

Team grant #2016ZT06S220. One of the datasets was provided by the Human Connectome Project, WU-Minn Consortium (Principal Investigators: David Van Essen and Kamil Ugurbil; 1U54MH091657) funded by the 16 NIH Institutes and Centers that support the NIH Blueprint for Neuroscience Research; and by the McDonnell Center for Systems Neuroscience at Washington University. We thank Dr. Li-Xia Yuan (Assistant researcher of Hangzhou Normal University) for her help on data analysis.

Code and data availability

Codes supporting this study are freely available at the GitHub repository (https://github.com/Cynthia1229/mfSD-DC). Data from HCP is publicly available at https://db.humanconnectome.org/. The Beijing and Hangzhou datasets are available from the corresponding author upon reasonable request. Sharing and re-use of the datasets require a formal data sharing agreement, as well as approval from the relevant Institutional Review Boards.

Ethics statement

The reanalysis of the Human Connectome Project (HCP) Open Access and Restricted Data and the reporting of results pertaining to this dataset had been reviewed and approved by the Beijing Normal University Institutional Review Board. The collection and analysis of the Beijing sample data was approved by the Institutional Review Board at Beijing Normal University. The collection and analysis of Hangzhou sample data was approved by the Ethics Committee of the Sir Run Run Shaw Hospital, School of Medicine, Zhejiang University, and the Affiliated Hospital of Hangzhou Normal University.

Supplementary materials

Supplementary material associated with this article can be found, in the online version, at doi:10.1016/j.neuroimage.2021.118187.

References

Achard, S., Salvador, R., Whitcher, B., Suckling, J., Bullmore, E., 2006. A resilient, low-frequency, small-world human brain functional network with highly connected association cortical hubs. J. Neurosci. 26, 63–72.

Alavash, M., Lim, S.J., Thiel, C., Sehm, B., Deserno, L., Obleser, J., 2018. Dopaminergic modulation of hemodynamic signal variability and the functional connectome during cognitive performance. Neuroimage 172, 341–356.

Armbruster-Genc, D.J., Ueltzhoffer, K., Fiebach, C.J., 2016. Brain signal variability differentially affects cognitive flexibility and cognitive stability. J. Neurosci. 36, 3978–3987.

Autio, J.A., Glasser, M.F., Ose, T., Donahue, C.J., Bastiani, M., Ohno, M., Kawabata, Y., Urushibata, Y., Murata, K., Nishigori, K., Yamaguchi, M., Hori, Y., Yoshida, A., Go, Y., Coalson, T.S., Jbabdi, S., Sotiropoulos, S.N., Kennedy, H., Smith, S., Van Essen, D.C., Hayashi, T., 2020. Towards HCP-Style macaque connectomes: 24-Channel 3T multi--array coil, MRI sequences and preprocessing. Neuroimage 215, 116800.

Bandettini, P.A., Wong, E.C., Jesmanowicz, A., Hinks, R.S., Hyde, J.S., 1994. Spin-echo and gradient-echo epi of human brain activation using bold contrast: a comparative study at 1.5 T. NMR Biomed. 7, 12–20.

Birn, R.M., Diamond, J.B., Smith, M.A., Bandettini, P.A., 2006. Separating respiratory-variation-related fluctuations from neuronal-activity-related fluctuations in fMRI. Neuroimage 31, 1536–1548.

Biswal, B., Zerrin Yetkin, F., Haughton, V.M., Hyde, J.S., 1995. Functional connectivity in the motor cortex of resting human brain using echo-planar MRI. Magn. Reson. Med. 34, 537–541.

Buckner, R.L., Sepulcre, J., Talukdar, T., Krienen, F.M., Liu, H., Hedden, T., Andrews-Hanna, J.R., Sperling, R.A., Johnson, K.A., 2009. Cortical hubs revealed by intrinsic functional connectivity: mapping, assessment of stability, and relation to Alzheimer's disease. J. Neurosci. 29, 1860–1873.

Bullmore, E., Sporns, O., 2009. Complex brain networks: graph theoretical analysis of structural and functional systems. Nat. Rev. Neurosci. 10, 186–198.

Caballero-Gaudes, C., Reynolds, R.C., 2017. Methods for cleaning the BOLD fMRI signal. Neuroimage 154, 128–149.

Cao, M., He, Y., Dai, Z., Liao, X., Jeon, T., Ouyang, M., Chalak, L., Bi, Y., Rollins, N., Dong, Q.J.C.C., 2017. Early development of functional network segregation revealed by connectomic analysis of the preterm human. brain 27, 1949–1963.

Chan, R.W., Leong, A.T.L., Ho, L.C., Gao, P.P., Wong, E.C., Dong, C.M., Wang, X., He, J., Chan, Y.S., Lim, L.W., Wu, E.X., 2017. Low-frequency hippocampal–cortical activity drives brain-wide resting-state functional MRI connectivity. Proc. Natl. Acad. Sci. 114, E6972.

Chen, X., Lu, B., Yan, C.G., 2018. Reproducibility of R-fMRI metrics on the impact of different strategies for multiple comparison correction and sample sizes. Hum. Brain Mapp. 39, 300–318.

Colasanti, A., Guo, Q., Giannetti, P., Wall, M.B., Newbould, R.D., Bishop, C., Onega, M., Nicholas, R., Ciccarelli, O., Muraro, P.A., Malik, O., Owen, D.R., Young, A.H., Gunn, R.N., Piccini, P., Matthews, P.M., Rabiner, E.A., 2016. Hippocampal neuroinflammation, functional connectivity, and depressive symptoms in multiple sclerosis. Biol. Psychiatry 80, 62–72.

Cox, R.W., 1996. AFNI: software for analysis and visualization of functional magnetic resonance neuroimages. Comput. Biomed. Res. 29, 162–173.

Damoiseaux, J.S., 2017. Effects of aging on functional and structural brain connectivity. Neuroimage 160, 32–40.

Damoiseaux, J.S., Rombouts, S.A., Barkhof, F., Scheltens, P., Stam, C.J., Smith, S.M., Beckmann, C.F., 2006. Consistent resting-state networks across healthy subjects. Proc. Natl. Acad. Sci. U. S. A. 103, 13848–13853.

Dennis, E.L., Thompson, P.M., 2014. Functional brain connectivity using fMRI in aging and Alzheimer's disease. Neuropsychol. Rev. 24, 49–62.

Di, X., Kim, E.H., Huang, C.C., Tsai, S.J., Lin, C.P., Biswal, B.B., 2013. The influence of the amplitude of low-frequency fluctuations on resting-state functional connectivity. Front. Hum. Neurosci. 7, 118.

Duan, J., Xia, M., Womer, F.Y., Chang, M., Yin, Z., Zhou, Q., Zhu, Y., Liu, Z., Jiang, X., Wei, S.J.H.b.m., 2019. Dynamic changes of functional segregation and integration in vulnerability and resilience to schizophrenia. Hum. Brain Mapp. 40, 2200–2211.

Evans, J.W., Kundu, P., Horovitz, S.G., Bandettini, P.A., 2015. Separating slow BOLD from non-BOLD baseline drifts using multi-echo fMRI. Neuroimage 105, 189–197.

Fan, L., Li, H., Zhuo, J., Zhang, Y., Wang, J., Chen, L., Yang, Z., Chu, C., Xie, S., Laird, A.R., Fox, P.T., Eickhoff, S.B., Yu, C., Jiang, T., 2016. The human brainnetome atlas: a new brain atlas based on connectional architecture. Cereb. Cortex 26, 3508–3526.

Feng, J., Chen, C., Cai, Y., Ye, Z., Feng, K., Liu, J., Zhang, L., Yang, Q., Li, A., Sheng, J., Zhu, B., Yu, Z., Chen, C., Dong, Q., Xue, G., 2020. Partitioning heritability analyses unveil the genetic architecture of human brain multidimensional functional connectivity patterns. Hum. Brain Mapp. 41, 3305–3317.

Ferreira, L.K., Busatto, G.F., 2013. Resting-state functional connectivity in normal brain aging. Neurosci. Biobehav. Rev. 37, 384–400.

Fornito, A., Harrison, B.J., Zalesky, A., Simons, J.S., 2012. Competitive and cooperative dynamics of large-scale brain functional networks supporting recollection. Proc. Natl. Acad. Sci. U. S. A. 109, 12788–12793.

Fox, M.D., Zhang, D., Snyder, A.Z., Raichle, M.E., 2009. The global signal and observed anticorrelated resting state brain networks. J. Neurophysiol. 101, 3270–3283.

Garrett, D.D., Epp, S.M., Perry, A., Lindenberger, U., 2018. Local temporal variability reflects functional integration in the human brain. Neuroimage 183, 776–787.

Garrett, D.D., Kovacevic, N., McIntosh, A.R., Grady, C.L., 2010. Blood oxygen level-dependent signal variability is more than just noise. J. Neurosci. 30, 4914–4921.

Garrett, D.D., Kovacevic, N., McIntosh, A.R., Grady, C.L., 2011. The importance of being variable. J. Neurosci. 31, 4496–4503.

Garrett, D.D., Kovacevic, N., McIntosh, A.R., Grady, C.L., 2013a. The modulation of BOLD variability between cognitive states varies by age and processing speed. Cereb. Cortex 23, 684–693.

Garrett, D.D., Lindenberger, U., Hoge, R.D., Gauthier, C.J., 2017. Age differences in brain signal variability are robust to multiple vascular controls. Sci. Rep. 7, 10149.

Garrett, D.D., McIntosh, A.R., Grady, C.L., 2014. Brain signal variability is parametrically modifiable. Cereb. Cortex 24, 2931–2940.

Garrett, D.D., Nagel, I.E., Preuschhof, C., Burzynska, A.Z., Marchner, J., Wiegert, S., Jungehulsing, G.J., Nyberg, L., Villringer, A., Li, S.C., Heekeren, H.R., Backman, L., Lindenberger, U., 2015. Amphetamine modulates brain signal variability and working memory in younger and older adults. Proc. Natl. Acad. Sci. U. S. A. 112, 7593–7598.

Garrett, D.D., Samanez-Larkin, G.R., MacDonald, S.W., Lindenberger, U., McIntosh, A.R., Grady, C.L., 2013b. Moment-to-moment brain signal variability: a next frontier in human brain mapping? Neurosci. Biobehav. Rev. 37, 610–624.

Glasser, M.F., Sotiropoulos, S.N., Wilson, J.A., Coalson, T.S., Fischl, B., Andersson, J.L., Xu, J., Jbabdi, S., Webster, M., Polimeni, J.R., Van Essen, D.C., Jenkinson, M., Consortium, W.U.M.H., 2013. The minimal preprocessing pipelines for the Human Connectome Project. Neuroimage 80, 105–124.

Greicius, M.D., Supekar, K., Menon, V., Dougherty, R.F., 2009. Resting-state functional connectivity reflects structural connectivity in the default mode network. Cereb. Cortex 19, 72–78.

Griffanti, L., Douaud, G., Bijsterbosch, J., Evangelisti, S., Alfaro-Almagro, F., Glasser, M.F., Duff, E.P., Fitzgibbon, S., Westphal, R., Carone, D., Beckmann, C.F., Smith, S.M., 2017. Hand classification of fMRI ICA noise components. Neuroimage 154, 188–205.

Griffanti, L., Salimi-Khorshidi, G., Beckmann, C.F., Auerbach, E.J., Douaud, G., Sexton, C.E., Zsoldos, E., Ebmeier, K.P., Filippini, N., Mackay, C.E., Moeller, S., Xu, J., Yacoub, E., Baselli, G., Ugurbil, K., Miller, K.L., Smith, S.M., 2014. ICA-based artefact removal and accelerated fMRI acquisition for improved resting state network imaging. Neuroimage 95, 232–247.

Guitart-Masip, M., Salami, A., Garrett, D., Rieckmann, A., Lindenberger, U., Backman, L., 2016. BOLD variability is related to dopaminergic neurotransmission and cognitive aging. Cereb. Cortex 26, 2074–2083.

He, Y., Chen, Z.J., Evans, A.C., 2007. Small-world anatomical networks in the human brain revealed by cortical thickness from MRI. Cereb. Cortex 17, 2407–2419.

He, Y., Wang, J., Wang, L., Chen, Z.J., Yan, C., Yang, H., Tang, H., Zhu, C., Gong, Q., Zang, Y., 2009. Uncovering intrinsic modular organization of spontaneous brain activity in humans. PLoS One 4, e5226.

Holm, S., 1979. A simple sequentially rejective multiple test procedure. Scandinavian journal of statistics 65–70.

Honey, C.J., Sporns, O., Cammoun, L., Gigandet, X., Thiran, J.P., Meuli, R., Hagmann, P., 2009. Predicting human resting-state functional connectivity from structural connectivity. Proc. Natl. Acad. Sci. U. S. A. 106, 2035–2040.
Hu, W.T., Wang, Z., Lee, V.M.Y., Trojanowski, J.Q., Detre, J.A., Grossman, M., 2010. Distinct cerebral perfusion patterns in FTLD and AD. Neurology 75, 881–888.
Kannurpatti, S.S., Biswal, B.B., 2008. Detection and scaling of task-induced fMRI-BOLD response using resting state fluctuations. Neuroimage 40, 1567–1574.
Kelly, C., de Zubicaray, G., Di Martino, A., Copland, D.A., Reiss, P.T., Klein, D.F., Castellanos, F.X., Milham, M.P., McMahon, K., 2009. L-dopa modulates functional connectivity in striatal cognitive and motor networks: a double-blind placebo-controlled study. J. Neurosci. 29, 7364–7378.
Khan, S., Gramfort, A., Shetty, N.R., Kitzbichler, M.G., Ganesan, S., Moran, J.M., Lee, S.M., Gabrieli, J.D., Tager-Flusberg, H.B., Joseph, R.M., Herbert, M.R., Hamalainen, M.S., Kenet, T., 2013. Local and long-range functional connectivity is reduced in concert in autism spectrum disorders. Proc. Natl. Acad. Sci. U. S. A. 110, 3107–3112.
Kielar, A., Deschamps, T., Chu, R.K., Jokel, R., Khatamian, Y.B., Chen, J.J., Meltzer, J.A., 2016. Identifying dysfunctional cortex: dissociable effects of stroke and aging on resting state dynamics in MEG and fMRI. Front. Aging Neurosci. 8, 40.
Kublbock, M., Woletz, M., Hoflich, A., Sladky, R., Kranz, G.S., Hoffmann, A., Lanzenberger, R., Windischberger, C., 2014. Stability of low-frequency fluctuation amplitudes in prolonged resting-state fMRI. Neuroimage 103, 249–257.
Kundu, P., Inati, S.J., Evans, J.W., Luh, W.M., Bandettini, P.A., 2012. Differentiating BOLD and non-BOLD signals in fMRI time series using multi-echo EPI. Neuroimage 60, 1759–1770.
Liang, X., Zou, Q., He, Y., Yang, Y., 2013. Coupling of functional connectivity and regional cerebral blood flow reveals a physiological basis for network hubs of the human brain. Proc. Natl. Acad. Sci. U. S. A. 110, 1929–1934.
Lindquist, M.A., Geuter, S., Wager, T.D., Caffo, B.S., 2019. Modular preprocessing pipelines can reintroduce artifacts into fMRI data. Hum. Brain Mapp. 40, 2358–2376.
Liu, F., Zhu, C., Wang, Y., Guo, W., Li, M., Wang, W., Long, Z., Meng, Y., Cui, Q., Zeng, L., Gong, Q., Zhang, W., Chen, H., 2015. Disrupted cortical hubs in functional brain networks in social anxiety disorder. Clin. Neurophysiol. 126, 1711–1716.
Liu, M., Song, C., Liang, Y., Knöpfel, T., Zhou, C., 2019. Assessing spatiotemporal variability of brain spontaneous activity by multiscale entropy and functional connectivity. Neuroimage 198, 198–220.
McDonough, I.M., Nashiro, K., 2014. Network complexity as a measure of information processing across resting-state networks: evidence from the Human Connectome Project. Front. Hum. Neurosci. 8, 409.
McDonough, I.M., Siegel, J.T., 2018. The relation between white matter microstructure and network complexity: implications for processing efficiency. Front. Integr. Neurosci. 12, 43.
McIntosh, A.R., Kovacevic, N., Itier, R.J., 2008. Increased brain signal variability accompanies lower behavioral variability in development. PLoS Comput. Biol. 4, e1000106.
McIntosh, A.R., Vakorin, V., Kovacevic, N., Wang, H., Diaconescu, A., Protzner, A.B., 2014. Spatiotemporal dependency of age-related changes in brain signal variability. Cereb. Cortex 24, 1806–1817.
Menon, R.S., Ogawa, S., Tank, D.W., Uğurbil, K., 1993. 4 Tesla gradient recalled echo characteristics of photic stimulation-induced signal changes in the human primary visual cortex. Magn. Reson. Med. 30, 380–386.
Misic, B., Vakorin, V.A., Paus, T., McIntosh, A.R., 2011. Functional embedding predicts the variability of neural activity. Front. Syst. Neurosci. 5, 90.
Murphy, K., Birn, R.M., Handwerker, D.A., Jones, T.B., Bandettini, P.A., 2009. The impact of global signal regression on resting state correlations: are anti-correlated networks introduced? Neuroimage 44, 893–905.
Nagano-Saito, A., Leyton, M., Monchi, O., Goldberg, Y.K., He, Y., Dagher, A., 2008. Dopamine depletion impairs frontostriatal functional connectivity during a set-shifting task. J. Neurosci. 28, 3697–3706.
Nomi, J.S., Bolt, T.S., Ezie, C.E.C., Uddin, L.Q., Heller, A.S., 2017. Moment-to-moment BOLD signal variability reflects regional changes in neural flexibility across the lifespan. J. Neurosci. 37, 5539–5548.
Ogawa, S., Lee, T.M., Kay, A.R., Tank, D.W., 1990. Brain magnetic resonance imaging with contrast dependent on blood oxygenation. Proc. Natl. Acad. Sci. 87, 9868–9872.
Petracca, M., Saiote, C., Bender, H.A., Arias, F., Farrell, C., Magioncalda, P., Martino, M., Miller, A., Northoff, G., Lublin, F., Inglese, M., 2017. Synchronization and variability imbalance underlie cognitive impairment in primary-progressive multiple sclerosis. Sci. Rep. 7, 46411.
Power, J.D., Barnes, K.A., Snyder, A.Z., Schlaggar, B.L., Petersen, S.E., 2012. Spurious but systematic correlations in functional connectivity MRI networks arise from subject motion. Neuroimage 59, 2142–2154.
Power, J.D., Cohen, A.L., Nelson, S.M., Wig, G.S., Barnes, K.A., Church, J.A., Vogel, A.C., Laumann, T.O., Miezin, F.M., Schlaggar, B.L., Petersen, S.E., 2011. Functional network organization of the human brain. Neuron 72, 665–678.
Power, J.D., Plitt, M., Gotts, S.J., Kundu, P., Voon, V., Bandettini, P.A., Martin, A., 2018. Ridding fMRI data of motion-related influences: Removal of signals with distinct spatial and physical bases in multiecho data. Proc. Natl. Acad. Sci. U. S. A. 115, E2105–E2114.
Power, J.D., Schlaggar, B.L., Petersen, S.E., 2015. Recent progress and outstanding issues in motion correction in resting state fMRI. Neuroimage 105, 536–551.
Salimi-Khorshidi, G., Douaud, G., Beckmann, C.F., Glasser, M.F., Griffanti, L., Smith, S.M., 2014. Automatic denoising of functional MRI data: combining independent component analysis and hierarchical fusion of classifiers. Neuroimage 90, 449–468.
Sato, J.R., Biazoli, C.E., Moura, L.M., Crossley, N., Zugman, A., Picon, F.A., Hoexter, M.Q., Amaro, E., Miguel, E.C., Rohde, L.A., Bressan, R.A., Jackowski, A.P., 2019. Association between fractional amplitude of low-frequency spontaneous fluctuation and degree centrality in children and adolescents. Brain Connect. 9, 379–387.
Satterthwaite, T.D., Wolf, D.H., Loughead, J., Ruparel, K., Elliott, M.A., Hakonarson, H., Gur, R.C., Gur, R.E., 2012. Impact of in-scanner head motion on multiple measures of functional connectivity: relevance for studies of neurodevelopment in youth. Neuroimage 60, 623–632.
Scarapicchia, V., Mazerolle, E.L., Fisk, J.D., Ritchie, L.J., Gawryluk, J.R., 2018. Resting state BOLD variability in Alzheimer's disease: a marker of cognitive decline or cerebrovascular status? Front. Aging Neurosci. 10, 39.
Sha, Z., Xia, M., Lin, Q., Cao, M., Tang, Y., Xu, K., Song, H., Wang, Z., Wang, F., Fox, P.T., Evans, A.C., He, Y., 2018. Meta-connectomic analysis reveals commonly disrupted functional architectures in network modules and connectors across brain disorders. Cereb. Cortex 28, 4179–4194.
Shafiei, G., Zeighami, Y., Clark, C.A., Coull, J.T., Nagano-Saito, A., Leyton, M., Dagher, A., Misic, B., 2019. Dopamine signaling modulates the stability and integration of intrinsic brain networks. Cereb. Cortex 29, 397–409.
Sheng, J., Shen, Y., Qin, Y., Zhang, L., Jiang, B., Li, Y., Xu, L., Chen, W., Wang, J., 2018. Spatiotemporal, metabolic, and therapeutic characterization of altered functional connectivity in major depressive disorder. Hum. Brain Mapp. 39, 1957–1971.
Shine, J.M., Aburn, M.J., Breakspear, M., Poldrack, R.A., 2018. The modulation of neural gain facilitates a transition between functional segregation and integration in the brain. Elife 7, e31130.
Shrout, P.E., Fleiss, J.L., 1979. Intraclass correlations: uses in assessing rater reliability. Psychol. Bull. 86, 420–428.
Smith, S.M., Beckmann, C.F., Andersson, J., Auerbach, E.J., Bijsterbosch, J., Douaud, G., Duff, E., Feinberg, D.A., Griffanti, L., Harms, M.P., Kelly, M., Laumann, T., Miller, K.L., Moeller, S., Petersen, S., Power, J., Salimi-Khorshidi, G., Snyder, A.Z., Vu, A.T., Woolrich, M.W., Xu, J., Yacoub, E., Ugurbil, K., Van Essen, D.C., Glasser, M.F., Consortium, W.U.M.H., 2013. Resting-state fMRI in the Human Connectome Project. Neuroimage 80, 144–168.
Sporns, O., 2013. Network attributes for segregation and integration in the human brain. Curr. Opin. Neurobiol. 23, 162–171.
Sporns, O., Honey, C.J., Kötter, R., 2007. Identification and classification of hubs in brain networks. PLoS One 2, e1049.
Team, R.C., 2020. R: A Language and Environment for Statistical Computing. R Foundation for Statistical Computing, Vienna, Austria.
Tomasi, D., Shokri-Kojori, E., Volkow, N.D., 2016. Temporal changes in local functional connectivity density reflect the temporal variability of the amplitude of low frequency fluctuations in gray matter. PLoS One 11, e0154407.
Tomasi, D., Volkow, N.D., 2018. Association between brain activation and functional connectivity. Cereb. Cortex.
Tomasi, D., Wang, G.J., Volkow, N.D., 2013. Energetic cost of brain functional connectivity. Proc. Natl. Acad. Sci. 110, 13642–13647.
Toulmin, H., Beckmann, C.F., O'Muircheartaigh, J., Ball, G., Nongena, P., Makropoulos, A., Ederies, A., Counsell, S.J., Kennea, N., Arichi, T., Tusor, N., Rutherford, M.A., Azzopardi, D., Gonzalez-Cinca, N., Hajnal, J.V., Edwards, A.D., 2015. Specialization and integration of functional thalamocortical connectivity in the human infant. Proc Natl Acad Sci U S A 112, 6485–6490.
Vakorin, V.A., Lippe, S., McIntosh, A.R., 2011. Variability of brain signals processed locally transforms into higher connectivity with brain development. J. Neurosci. 31, 6405–6413.
Van Essen, D.C., Smith, S.M., Barch, D.M., Behrens, T.E., Yacoub, E., Ugurbil, K., Consortium, W.U.M.H., 2013. The WU-Minn human connectome project: an overview. Neuroimage 80, 62–79.
Wang, D.J.J., Jann, K., Fan, C., Qiao, Y., Zang, Y.F., Lu, H., Yang, Y., 2018. Neurophysiological basis of multi-scale entropy of brain complexity and its relationship with functional connectivity. Front. Neurosci. 12, 352.
Wang, J., Wang, X., Xia, M., Liao, X., Evans, A., He, Y., 2015. GRETNA: a graph theoretical network analysis toolbox for imaging connectomics. Front. Hum. Neurosci. 9, 386.
Wang, Z., Aguirre, G.K., Rao, H., Wang, J., Fernández-Seara, M.A., Childress, A.R., Detre, J.A., 2008. Empirical optimization of ASL data analysis using an ASL data processing toolbox: ASLtbx. Magn. Reson. Imaging 26, 261–269.
Winkler, A.M., Ridgway, G.R., Douaud, G., Nichols, T.E., Smith, S.M., 2016. Faster permutation inference in brain imaging. Neuroimage 141, 502–516.
Wu, C.W., Gu, H., Lu, H., Stein, E.A., Chen, J.H., Yang, Y., 2009. Mapping functional connectivity based on synchronized CMRO2 fluctuations during the resting state. Neuroimage 45, 694–701.
Xiong, J., Gao, J.H., Lancaster, J.L., Fox, P.T., 1995. Clustered pixels analysis for functional MRI activation studies of the human brain. Hum. Brain Mapp. 3, 287–301.
Yan, C.G., Yang, Z., Colcombe, S.J., Zuo, X.N., Milham, M.P., 2017. Concordance among indices of intrinsic brain function: Insights from inter-individual variation and temporal dynamics. Sci. Bull. 62, 1572–1584.
Yan, C.G., Chen, X., Li, L., Castellanos, F.X., Bai, T.J., Bo, Q.J., Cao, J., Chen, G.M., Chen, N.X., Chen, W., Cheng, C., Cheng, Y.Q., Cui, X.L., Duan, J., Fang, Y.R., Gong, Q.Y., Guo, W.B., Hou, Z.H., Hu, L., Kuang, L., Li, F., Li, K.M., Li, T., Liu, Y.S., Liu, Z.N., Long, Y.C., Luo, Q.H., Meng, H.Q., Peng, D.H., Qiu, H.T., Qiu, J., Shen, Y.D., Shi, Y.S., Wang, C.Y., Wang, F., Wang, K., Wang, L., Wang, X., Wang, Y., Wu, X.P., Wu, X.R., Xie, C.M., Xie, G.R., Xie, H.Y., Xie, P., Xu, X.F., Yang, H., Yang, J., Yao, J.S., Yao, S.Q., Yin, Y.Y., Yuan, Y.G., Zhang, A.X., Zhang, H., Zhang, K.R., Zhang, L., Zhang, Z.J., Zhou, R.B., Zhou, Y.T., Zhu, J.J., Zou, C.J., Si, T.M., Zuo, X.N., Zhao, J.P., Zang, Y.F., 2019. Reduced default mode network functional connectivity in patients with recurrent major depressive disorder. Proc. Natl. Acad. Sci. U. S. A. 116, 9078–9083.
Yan, C.G., Wang, X.D., Zuo, X.N., Zang, Y.F., 2016. DPABI: data processing & analysis for (resting-state) brain imaging. Neuroinformatics 14, 339–351.
Yeo, B.T., Krienen, F.M., Sepulcre, J., Sabuncu, M.R., Lashkari, D., Hollinshead, M., Roffman, J.L., Smoller, J.W., Zollei, L., Polimeni, J.R., Fischl, B., Liu, H., Buckner, R.L.,

2011. The organization of the human cerebral cortex estimated by intrinsic functional connectivity. J. Neurophysiol. 106, 1125–1165.
Zang, Y.F., He, Y., Zhu, C.Z., Cao, Q.J., Sui, M.Q., Liang, M., Tian, L.X., Jiang, T.Z., Wang, Y.F., 2007. Altered baseline brain activity in children with ADHD revealed by resting-state functional MRI. Brain Dev. 29, 83–91.
Zoller, D., Schaer, M., Scariati, E., Padula, M.C., Eliez, S., Van De Ville, D., 2017. Disentangling resting-state BOLD variability and PCC functional connectivity in 22q11.2 deletion syndrome. Neuroimage 149, 85–97.
Zou, Q.H., Zhu, C.Z., Yang, Y., Zuo, X.N., Long, X.Y., Cao, Q.J., Wang, Y.F., Zang, Y.F., 2008. An improved approach to detection of amplitude of low-frequency fluctuation (ALFF) for resting-state fMRI: fractional ALFF. J. Neurosci. Methods 172, 137–141.
Zuo, X.N., Di Martino, A., Kelly, C., Shehzad, Z.E., Gee, D.G., Klein, D.F., Castellanos, F.X., Biswal, B.B., Milham, M.P., 2010. The oscillating brain: complex and reliable. Neuroimage 49, 1432–1445.
Zuo, X.N., Xing, X.X., 2014. Test-retest reliabilities of resting-state FMRI measurements in human brain functional connectomics: a systems neuroscience perspective. Neurosci. Biobehav. Rev. 45, 100–118.